Title: **The mechanisms of *in vivo* commensal control of *Clostridioides difficile* virulence**

Authors: Girinathan BP[1*], DiBenedetto N[1*], Worley J[1,2], Peltier J[3§], Lavin R[4], Delaney ML[1,5], Cummins C[1], Onderdonk AB[1,5], Gerber GK[1,6,], Dupuy B[3], Sonenshein AL[4], Bry L[1,5,**]

Abstract:

We define multiple mechanisms by which commensals protect against or worsen *Clostridioides difficile* infection. Using a systems-level approach we show how two species of *Clostridia* with distinct metabolic capabilities modulate the pathogen's virulence to impact host survival. Gnotobiotic mice colonized with the amino acid fermenter *Clostridium bifermentans* survived infection, while colonization with the butyrate-producer, *Clostridium sardiniense,* more rapidly succumbed. Systematic *in vivo* analyses revealed how each commensal altered the pathogen's carbon source metabolism, cellular machinery, stress responses, and toxin production. Protective effects were replicated in infected conventional mice receiving *C. bifermentans* as an oral bacteriotherapeutic that prevented lethal infection. Leveraging a systematic and organism-level approach to host-commensal-pathogen interactions *in vivo,* we lay the groundwork for mechanistically-informed therapies to treat and prevent this disease.

Author Affiliations:

1. Massachusetts Host-Microbiome Center, Dept. Pathology, Brigham & Women's Hospital, Harvard Medical School, Boston, MA
2. National Center of Biocomputing Information, National Library of Medicine, Bethesda, MD
3. Laboratory of the Pathogenesis of Bacterial Anaerobes, Institut Pasteur, Université de Paris, France
4. Department of Molecular Biology and Microbiology, Tufts University School of Medicine, Boston, MA
5. Clinical Microbiology Laboratory, Department of Pathology, Brigham & Women's Hospital, Harvard Medical School, Boston, MA
6. Harvard-MIT Health Sciences & Technology, Boston, MA

* These authors contributed equally to the studies undertaken.
**Communicating Author: Lynn Bry, MD, PhD; lbry@bwh.harvard.edu
§ Present address: Institute for Integrative Biology of the Cell (I2BC), CEA, CNRS, Univ. Paris-Sud, Université Paris-Saclay, 91198, Gif-sur-Yvette cedex, France

Introduction

Clostridioides difficile, the etiology of pseudomembranous colitis, causes substantantial morbidity, mortality and >$5 billion/year in US healthcare costs. Infections commonly arise after antibiotic disruption of the microbiota, allowing the pathogen to proliferate and release toxins that ADP ribosylate host rho GTPases (*1, 2*). In patients with recurrent *C. difficile* infections, fecal microbiota transplant (FMT) has become standard of care to reconstitute the microbiota and prevent recurrence. While intensive efforts to develop defined microbial replacements for FMT have been undertaken, relatively little is known about the molecular, metabolic, and microbiologic mechanisms by which specific members of the microbiota modulate the pathogen's virulence *in vivo,* information critical for therapeutics development (*3, 4*). Given deaths in immunocompromised patients from drug-resistant pathogens in FMT preparations (*5*), therapies informed by molecular mechanisms of action among will enable options with improved safety and efficacy (*6, 7*).

C. difficile's pathogenicity locus (PaLoc) contains the *tcdA, tcdB* and *tcdE* genes that encode the A and B toxins, and holin involved in toxin export, respectively. *tcdR* encodes a sigma factor specific for the toxin gene promoters, and the *tcdC* gene a TcdR anti-sigma factor (*8-10*). Multiple metabolic regulators influence PaLoc expression (*11, 12*). In particular, *C. difficile* elaborates toxin under starvation conditions to extract nutrients from the host and promote the shedding of spores.

C. difficile, like other cluster XI *Clostridia*, possesses diverse genetic machinery to utilize different carbon sources for energy and growth. In addition to carbohydrate fermentation, the pathogen uses Stickland fermentations, and Stickland-independent fermentations of other amino acids including threonine and cysteine (*13*), to extract energy from amino acids. The pathogen can ferment ethanolamine, extract electrons from primary bile salts, and undergo carbon fixation through the Wood-Ljungdhal pathway to generate acetate for metabolism or biosynthetic pathways (*11, 14*).

Metabolic regulators within *C. difficile*, including CodY, CcpA, PrdR, and Rex sense intracellular levels of GTP, branched-chain amino acids, fructose 1,6 bis-phosphate, and proline – the dominant Stickland acceptor amino acid, or NAD^+/NADH pools respectively (*12, 15*). Under conditions of nutrient sufficiency these regulators act coordinately through direct and indirect mechanisms to repress PaLoc expression. Starvation or other drivers of metabolic stress reduce each regulator's repression of the PaLoc and, in combination with positive regulators

including SigD, the flagellar sigma factor that contributes to *tcdR* transcription, RstA and LexA, can promote high levels of toxin production with severe disease (*16, 17*). Prior studies also identified the capacity of exogenous butyrate to induce *C. difficile* toxin expression, though mechanisms of action remain ill-defined (*18, 19*).

C. difficile also possesses multi-gene systems that promote lysis including diffocins, phage with lytic programs, and cell wall hydrolases that lyse the sporulating mother cell (*20-23*). Enrivonmental stressors, including nutrient limitation, quorum sensing of surrounding *C. difficile* populations, and other factors can induce these pathways to pomote abrupt release of toxin stores through TcdE-independent mechanisms. Furthermore, acute host responses including reactive oxygen species (ROS) and antimicrobial factors also stimulate the pathogen's expression of stress and lytic programs (*24, 25*).

The host and gut microbiota can thus impact the pathogen's physiology and toxin release through multiple mechanisms. Among Stickland-fermenting Cluster XI Clostridia, *Clostridium bifermentans* (CBI), a strongly proteolytic species, preferentially uses Stickland fermentations for energy extraction (*26*). In contrast, *Clostridium sardiniense* (CSAR), a non-Stickland fermenter and strongly glycolytic Cluster I *Clostridial* species, produces abundant butyrate through anaerobic carbohydrate fermentation (*26*). Both species colonize the human gut yet have very different metabolic capabilities.

Using defined-association experiments in gnotobiotic mice, we show mechanisms by which individual *Clostridial* species affect host survival of *C. difficile* infection, to the level of the microbial pathways and small molecules involved. Findings informed use of a defined bacteriotherapeutic to treat an already-infected conventional host. By defining how individual commensals modulate *C. difficile's* virulence we open new opportunities for mechanistically-informed approaches to treat and prevent this disease.

Results

Clostridium bifermentans protects gnotobiotic mice from lethal *C. difficile* infection while *Clostridium sardiniense* enhances disease severity.

C. difficile infection of 6 week old germfree mice caused rapid demise within 48h (Figs. 1A-B). Symptoms developed at 20h post-challenge with 1,000 *C. difficile* spores, manifested by weight loss (Figs. S1A-B), diarrhea, and worsening symptoms. Histologically, animals demonstrated initial focal epithelial damage with neutrophilic infiltrates in the large intestine (compare Figs. 1C vs 1D) that rapidly progressed over 24-48h to severe colitis with widespread erosions (Fig. S1C).

In contrast, mice pre-colonized with CBI prior to *C. difficile* challenge survived (Fig. 1B; $p<0.0001$) with milder colonic damage and acute weight loss (compare Figs. 1E vs S1D; Figs. S1A-B). Fourteen days after infection animals had regained lost weight and demonstrated intact intestinal epithelium with a lymphocytic infiltrate having replaced acute neutrophilic infiltrates (Fig. 1F).

Mice co-colonized with CSAR developed more rapidly lethal infection with *C. difficile* (Fig 1B; $p<0.0001$), with areas of epithelial sloughing and blood entering the lumen by 20h of infection (compare Figs. S1E vs. 1G), followed by widespread mucosal denudation and rapid demise (Fig. 1H).

Though toxin levels were comparable among mice at 20h of infection (Fig. 1I), pathogen vegetative and spore biomass in CSAR-co-colonized mice were 3-fold higher than in *C. difficile*-monocolonized or CBI-co-colonized mice (Fig. 1J-K). By 24h of infection *C. difficile*-monocolonized and CSAR-co-colonized mice demonstrated 2-3-fold higher toxin levels and vegetative biomas than CBI-co-colonized mice (Fig. 1I-J). Spore biomass in CBI-co-colonized mice at 24h was reduced 10-fold compared to the other conditions (Fig. 1K). After 14 days, toxin levels in surviving CBI-co-colonized mice fell >80% from levels seen acutely (Fig. 1I).

While CSAR biomass rose 10-fold (Fig S1F), CBI biomass did not change over acute infection (Fig. S1G). Commensal colonization also did not alter toxin integrity nor cytotoxic activity (Fig. 1L-M).

Commensals condition the gut nutrient environment prior to *C. difficile's* introduction.

Luminal substrates for microbial growth and metabolism originate from non-absorbed dietary components, primary host or microbial-origin compounds, and their metabolites (*27*). Given the effects of

commensal colonization on pathogen biomass, metabolomic analyses evaluated the nutrient content available to support *C. difficile* growth and metabolism (Fig. 2; Supplemental Data Files SDF1-2, Supplemental Text).

Germfree cecal contents were significantly enriched for multiple classes of fermentable amino acids (SDF_2.11, 2.24) and carbohydrates (SDF2.9, 2.12, 2.25), including sugar alcohols of dietary origin with poor absorption from mouse and human gut (*28*), and multiple purines and pyrimidines (Figs. 2A-G, SDF_2.17-2.19). In the absence of colonizing microbiota SCFA were absent (Fig. 2G).

Monoclonization with CSAR or with CBI markedly changed the luminal environment prior to *C. difficile's* introduction. CSAR-monocolonization enriched multiple amine-containing carbon sources (Fig 2A, top), including Stickland donor amino acids (SDF_2.24), additional fermentable amino acids (SDF_2.11) including cysteine, glutamate and asparate, which *C. difficile* can ferment in non-Stickland reactions (*11*), γ-glutamyl-amino acids (SDF_2.8), which originate from microbial metabolism and host amino acid transport (*29*), and di- and polyamines (SDF_2.3). Among these sources, branched chain amino acids increased >2-3-fold (Fig. 2C), and ornithine >16-fold over germfree levels (Fig. 2D).

Among carbohydrate sources, CSAR depleted lumenal fructose, left mannitol/sorbitol levels unchanged and enriched levels of amino sugars, including ones originating from host glycoconjugates (Fig. 2B). CSAR-monocolonization depleted multiple purines and pyrimidines (SDF_2.17-2.19) with >10-fold increases in 1-methylhypoxanthine and 1-methyladenine, metabolites reported in other purine-fermenting *Clostridia* (Fig. 3E; (*30*). Colonization also promoted substantive increases in 3-ureidopropionate, a metabolite of microbial uracil metabolism, and >10-fold increase in beta-alanine which can originate from decarbamoylation of 3-ureidopropionate (*31*) (Fig 3E; SDF_2.19). Primary SCFA fermentation metabolites included acetate and butyrate (Fig. 2G).

In contrast, CBI-monocolonization depleted polyamines, and Stickland acceptor and other fermentable amino acids (Fig. 2A, middle), consuming >70% of proline, >50% of glycine and >50% of threonine (Fig. 2D). CBI produced abundant 5-amino-valerate (Fig. 2F) from proline, and isocaproate from reductive leucine Stickland reactions (*32*) (Fig. 2G). From Stickland oxidative reactions, branched-SCFAs isobutyrate, isovalerate and 2-methylbutyrate were produced from branched-chain amino acids (Fig. 2G) and multiple aromatic amino acid metabolites from phenylalanine, tyrosine and tryptophan (Figs. S2A-B).

Among carbohydrates, CBI consumed >50% of fructose, left sugar alcohol levels unchanged (Fig 2B; SDF_2.25), and produced acetate and propionate but no detectable butyrate (Fig 2G). CBI-monocolonization depleted multiple luminal pyrimidines and xanthosines (SDF_2.17-2.19), and substantively increased levels of 1-methylhypoxanthine and 1-methyladenine (Fig 2E). 3-ureidopopionate increased to a lesser extent that seen in CSAR-monocolonized mice, and without increased levels of beta-alanine (Fig 3E; SDF_2.19).

C. difficile-monocolonzied mice demonstrated the broadest depletion of carbohydrate and amine-containing carbon sources (Fig 2A, bottom). The pathogen actively depleted Stickland acceptor- (Fig 2D), γ-glutamyl- (SDF_2.8), and other fermentable amino acids (SDF_2.11), consuming >70% of proline (Fig. 2D), with concomintant increase in 5-aminovalerate (Fig. 2F), and consuming >70% of threonine and >50% of glycine (Figs. 2F-G). γ-glutamyl- and N-acetyl amino acid conjugates to proline, branched-chain amino acids, and polyamines were also depleted (SDF_2.8, 2.10, 2.3).

Hexoses, pentoses and sugar alcohols were depleted, including >99% of luminal sorbitol/mannitol and >80% of fructose (Figs. 2A-B). In contrast to CSAR- and CBI-monocolonization, *C. difficile*-monocolonization did not show substantive depletion of purine or pyrimidine carbon sources but produced detectable 3-ureidopropionate (Fig. 2E, SDF_2.17-2.19).

C. difficile-monoclonization produced acetate (Fig. 2G), which arises from carbohydrate fermentation, Stickland glycine and alanine fermentation, Wood-Ljungdahl metabolism, and other cellular processes (*11*), and the Stickland branched-SCFA metabolites isobutyrate, isovalerate, 2-methylbutyrate and isocaproate (Fig. 2G). Aromatic amino acid and histidine metabolites specific to the pathogen's Stickland metabolism were also produced (Fig. S2A-B, Supplemental Text).

By 20h of infection, and per rapidly deteriorating mucosal conditions, CSAR and *C. difficile*-co-colonized mice (Fig 2H, top) demonstrated further enrichment of Stickland donor, acceptor, and other fermentable amino acids (Fig. 2C-D). Levels of uracil increased >8-fold and 3-ureidopropionate >40-fold compared to *C. difficile*-monocolonized mice (Fig. 3E; SDF_2.19). In contrast, CBI and *C. difficile*-co-colonized mice showed no differences in amine-containing carbon sources as compared to *C. difficile*-monoclonized mice (Fig. 2C-D). CBI-specific Stickland aromatic amino acid metabolites predominated in the co-coloinzed state, suggesting a

dominance of CBI's Stickland metabolism (Figs. S2A-B, Supplemental Text). These findings illustrated CSAR's capacity to create a nutrient enriched environment for *C. difficile* while CBI depleted many preferred nutrients.

Microbial colonization also altered levels of many host-origin compounds and of microbial metabolites with potential host effects. All three species enriched levels of host primary bile acids, including ones with *in vitro* inhibitory effects on *C. difficile* germination, such as β-muricholate and chenodeoxycholate, and others with simulatory effects including cholate and taurocholate (*33, 34*) (Fig 2A; SDF_2.16). *C. difficile*-monocolonized mice produced 7-ketodeoxycholate, a secondary bile acid (Supplemental Text) from the pathogen's 7α-hydroxysterol-dehydrogenase (*35*). Though CSAR carries a 7α-HSDH homolog enzyme (Supplemental Text), comparable changes were not observed in mice. CBI-monocolonization increased many host-origin sphingosine-containing compounds (SDF_2.22), while CBI- and CSAR-monocolonization each enriched compounds with host neurotransmitter activities, including metabolites with serotonergic, GABA-ergic or NMDA-ergic activites, or with additional anti-inflammatory properties such as ethanolamide endocannabinoids (Supplemental Text; SDF_2.1, 2.5) (*36*). These molecules were further enriched with the severe mucosal damage from CSAR and *C. difficile*-co-colonization.

CBI and CSAR differentially modulate *C. difficile* gene expression *in vivo.*

Commensal alterations in lumenal nutrient composition drove global alterations in *C. difficile* gene expression (Figs. 3A-E, SDF_4-5). Pathway enrichment analyses of *C. difficile*-monocolonized mice at 20h of infection showed significant enrichment of genes for the transport and metabolism of simple carbohydrates including glucose, fructose, ribose and disaccharides (Figs. 3A, 3D, SDF_5.2, 5.5, 5.7-9, 5.13), dipeptides and oligopeptides (SDF_5.4), and Wood-Ljungdahl pathway genes for CO2 fixation to acetate (SDF_5.17). By 24h the pathogen up-regulated ethanolamine utilization genes (SDF_5.6), enabling capacity to use ethanolamine and amino-alcohol lipids released from damaged mucosa (*14*).

With the amino acid and polyamine enrichment from CSAR-monocolonization, *C. difficile* in co-colonized mice up-regulated amino acid and polyamine transporters, Stickland reductases, particularly the proline and reductive leucine systems (Fig. 3A; Supplemental Text; SDF_5.14, 5.16), and pathways to convert CSAR-enriched ornithine to Stickland fermentable substrates. In this latter category, *C. difficile* enriched expression of

genes converting ornithine to alanine, and constitutively expressed genes converting ornithine to proline (Figs. 3C, S3A), enabling ornithine's use in both oxidative and reductive Stickland reactions (*37*). These effects co-occurred with CSAR's up-regulation of an arginine deiminase (ADI) fermentation pathway by 20h of *C. difficile* infection (Fig. S3B), including the *acrD* arginine:ornithine antiporter which exports the ornithine product of arginine fermentation, identifiying a cause for the significantly elevated ornithine in CSAR-monocolonized mice (*38*). In constrast, CBI's ADI pathway was down-regulated at 20h of co-colonization with *C. difficile*, followed by up-regulation by 24h with expression of its ornithine cyclodeaminase (OCD) which converts ornithine to proline, potentially conserving a proline-convertible carbon source for its Stickland metabolism (Figs. 3C, S3C).

With CSAR-co-colonization *C. difficile* also up-regulated a hydantoinase (Fig 3F, Supplemental Text) able to metabolize uracil to 3-ureidopropionate, given the significant enrichment of uracil in co-colonized mice (Fig. 2E).

With CBI-co-colonization (Fig. 3D-E), the pathogen adapted its metabolism to available nutrients, showing enrichment of genes to transport and metabolize sugar alcohols (SDF_5.15), including mannitol and sorbitol utilization operons, disaccharides (SDF_5.5), and polysaccharides (SDF_5.11), carbon sources not utilized by CBI (*26*). *C. difficile* also enriched expression of genes for the transport and metabolism of xanthines (*30*) concomitant with enrichment of these compounds during CBI-monoconolonization (SDF_5.18).

In the presence of either commensal, *C. difficile* down-regulated cobalamin biosynthesis genes (Figs. 3A-B, 3D-E; SDF_5.27), in addition to folate biosynthesis when co-colonized with CSAR (SDF_5.28), suggesting cross-feeding of these nutrients with co-colonization.

Commensal colonization profoundly altered the pathogen's cellular machinery. *C. difficile* genes associated with transcription, translation, and DNA replication were up-regulated with CSAR-co-colonization (Fig. 3A-B; SDF_5.20-5.23). In contrast, by 24h of infection in CBI-co-colonized mice, the pathogen profoundly down-regulated protein synthesis, including multi-gene systems for translation and ribosome production (Fig. 3E; SDF_5.21-5.22).

With the host's evolving inflammatory responses, commensal colonization also altered *C. difficile's* stress responses. By 20h of infection *C. difficile*-monocolonized mice enriched expression of CRISPR genes (SDF_5.38), diffocin lytic genes (Fig. 3A, D; SDF_5.39), a phage-like system induced by quorum sensing that

can lyse other *C. difficile* (*20*), and cell wall turnover enzymes (SDF_5.24). In CSAR-co-colonized mice, *C. difficile* sporulation pathways (SDF_5.42) and oxidative stress responses including superoxide dismutase (*sodA*), catalase (*cotG)* and nitroreductases were enriched (SDF_5.40), as were genes for terpenoid backbone synthesis (SDF_5.35), compounds in the spore coat and that can also provide anti-oxidant activities (*39*). In contrast, CBI-co-colonization showed depletion of diffocins (SDF_5.39) without enrichment of other stress response systems (Figs. 3D-E; SDF_5.38-5.42).

Each commensal differentially affected PaLoc expression. While toxin gene expression was comparable among conditions at 20h of infection (Figs. 3G-J), by 24h, *tcdA* and *tcdB* expression had increased *in C. difficile*-monocolonized mice (Figs. 3G-H). In contrast, in CBI-co-colonized mice, *tcdR* expression increased 12-fold (Fig. 3I), though *tcdB* and *tcdA* expression remained comparable to levels seen at 20h (Figs. 3G-H), and *tcdE* expression decreased (Fig. 3J). While CSAR-co-colonized mice showed reduced *tcdB* expression at 24h, these effects occurred in the context of higher pathogen vegetative biomass and toxin levels per gram of cecal contents than in *C. difficile*-monocolonized mice (Fig. 1I-J).

C. difficile infection also drove global alterations in commensal gene expression affecting each commensal's carbon source metabolism, cellular machinery, and induction of oxidative stress responses (Figs. S3D-G; SDF_6-7). These latter aspects of oxidative stress further modified electron transport and energy generating pathways for both commensals (Supplemental Text),

CBI protects against *C. difficile* mutants lacking the CodY and CcpA PaLoc metabolic repressors.

CcpA and CodY repress *C. difficile* toxin expression when intracellular pools of fructose 1,6 bis-phosphate, or branched-chain amino acids and GTP, respectively, indicate sufficient carbohydrate or Stickland fermentable substrates to support metabolism (*13, 40*). Given CBI's alterations on the gut nutrient environment and reduction of toxin levels, we evaluated whether these regulators mediated CBI's host-protective effects.

Δ*codY*, Δ*ccpA,* and double Δ*codY*Δ*ccpA C. difficile* mutants were each lethal in monocolonized mice while CBI-co-colonized mice survived (Figs. 4A, S4A-C). *In vivo* biomass and toxin studies identified CBI's effects on each mutant's growth and toxin production (Figs. 4B-D, S4D-F). CBI-co-colonized mice infected with the *ΔccpA* mutant demonstrated reduced *C. difficile* vegetative biomass and toxin levels at 16h (Figs. 4B-C, S4D-

E). At 24h of infection, toxin levels were comparable between colonization states with the mutant, and fell >80% by 14 days in surviving CBI-co-colonized mice (Fig. 4C).

In contrast, Δ*codY*-infected mice demonstrated better growth with CBI-co-colonization, while the double mutant grew poorly (Figs 4B, S4D). At 16h of infection the Δ*codY* mutant showed comparable vegetative biomass in monocolonized and co-colonized states, and elevated spore biomass in CBI-co-colonzied mice. The Δ*codY* mutant showed higher toxin levels at 16h as compared to wild-type controls, though levels in CBI-co-colonized mice were 70% lower that in Δ*codY*-monocolonized controls (Figs. 4C, S4E). However, from 16h to 24h, toxin levels fell >40-fold in CBI-co-colonized mice (Figs. 4D, S4E), in spite of the Δ*codY* mutant's higher vegetative biomass at 24h in co-colonized mice (Figs. 4B, S4D). These findings illustrated CBI's capacity to modulate the pathogen's growth, toxin production, and host survival, even in the absence of the PaLoc CodY and CcpA repressors.

CBI bacteriotherapy rescues conventional mice from lethal infection.

To assess CBI's potential as a therapeutic intervention, clindamycin-treated conventional mice were orally challenged with 1,000 *C. difficile* spores, followed by gavage at the onset of symptomatic infection with 10^8 CFU of CBI or vehicle-only control (Fig. 5A). 100% of CBI-treated mice survived while control-treated mice demonstrated 40% lethality (Figs. 5B, p=0.0061; S5A-C). At 30h post-*C. difficile* challenge, at the height of symptomatic infection, CBI-treated mice demonstrated reduced toxin levels and pathogen vegetative and spore biomass as compared to controls (Fig. 5C-E). By 14 days surviving mice had low to undetectable toxin levels (Fig 5C) and had largely cleared *C. difficile* and CBI (Figs. 5D-E; S5C). These findings validated CBI's therapeutic capacity in a conventional host when administered *after* the onset of symptomatic infection.

Carbon source enrichment analyses identified clindamycin's enrichment of multiple carbon sources including polyamines, Stickland acceptor- and γ-glutamyl-amino acids (Fig. 5F-G, SDF_10.4, 10.19, 10.8). Notably, the profiles of Stickland-fermentable amino acids and γ-glutamyl-amino acids in post-clindamycin treated mice clustered with those seen in CSAR-monocolonized mice (Fig. 5H-I; p<0.001), illustrating capacity for antibiotics and commensally-induced conditions to enable *C. difficile* growth and toxin production.

In vehicle-alone treated infected mice, the pathogen depleted disaccharides and oligosaccharides, pentoses, Stickland acceptor- and γ-glutamyl-amino acids (Fig. 5G top left-hand side; SDF_10.5, 10.19, 10.8, 10.19). With CBI-treatment, these and additional compounds in these categories, including galactinol and γ-glutamyl-glutamate were depleted (Fig. 5G, bottom; SDF_10.5, 10.8). Clindamycin treatment also depleted host ethanolamine endocannabinoids and sphingosines, compounds that demonstrated improved recovery in mice receiving CBI (Fig. 5G; SDF_10.6, 10.18).

Discussion

We demonstrate distinct mechanisms by which individual commensals modulate *C. difficile's* virulence *in vivo*. These findings have important implications to prevent and treat this disease, whether with targeted bacteriotherapeutics, small molecules, or other interventions, and to avoid conditions that pre-dispose patients to adverse outcomes such as toxic megacolon and recurrent infections. Importantly, FMT preparations of uncharacterized microbial populations can contain both protective and disease-exacerbating species. Introduced species may exihibit different behaviors near- and longer-term in antibiotic-depleted versus intact microbiota. The effects highlight the importance of leveraging mechanistic data to inform testing of patients and therapeutics for signals of efficacy and exacerbation, and to optimize defined microbial preparations for therapeutic effects.

Development and severity of *C. difficile* infection occurs as a function of the pathogen's biomass, toxin production, and duration to which host tissues are exposed to toxin. Using a tractable gnotobiotic infection model, we identified the remarkably protective effects of a single commensal species, *C. bifermentans,* against *C. difficile,* and capacity for another *Clostridial* species, *C. sardiniense,* to promote more rapidly severe disease.

Figure 6 illustrates the multiple mechanisms by which each commensal in combination with host responses modulated *C. difficile*'s virulence. Commensal colonization altered the gut nutrient environment prior to *C. difficile*'s introduction per consumption of fermentable carbon sources and enrichment or depletion of growth-supporting nutrients and metabolites.

Upon *C. difficile*'s introduction, commensal competition and nutrient availability impacted the pathogen's growth and induction of stress responses, including ones directly promoting toxin gene expression, and others such as diffocins and sporulation, that impacted cellular integrity and potential toxin release through TcdE-

independent mechanisms. *C. difficile*-monocolonized mice up-regulated diffocin genes, loci induced through quorum-sensing mechanisms where lysis of a portion of the population can release intracellular toxin stores to promote host damage and release nutrients for surviving vegetative populations (*20*). Sporulation also induced expression of cell wall hydrolases that lyse the mother cell. These mechanisms may enable abrupt and TcdE-independent release of intracellular toxin stores, a process known to occur in other toxigenic species such as *Shigella* and ETEC where antibiotics or induction of lysogenic phage can promote abrupt toxin release through cell disruption *(23, 41)*.

In response to CSAR's enrichment of amine-containing carbon sources *C. difficile* up-regulated multiple amino acid transporters, Stickland fermentation pathways, and genes to convert CSAR-enriched ornithine to Stickland-metabolizable substrates. Resulting biomass of *C. difficile* and CSAR expanded with the increased carrying capacity of the altered gut environment and, with further nutrient release from damaged tissues, created a positive-feedback loop for microbial growth and toxin production, resulting in a rapidly lethal infection. Notably, CSAR produces abundant butyrate, which has been shown to to induce toxin expression *in vitro* (*18*), while other*s* have suggested protective effects *in vivo* (*42*). Our studies showed that millimolar levels of microbial-origin butyrate did not prevent severe infection, rather multiple microbial mechanisms were involved in modulating pathogen behaviors and resulting host outcomes.

Notably, CSAR and CBI possess arginine deminase fermentation pathways, genes that modulated very different effects *in vivo* on *C. difficile's* growth and pathogenesis (Fig. 3C). With CSAR, the commensal's export of ornithine provided a new nutrient source for *C. difficile* metabolism and growth. In contrast, CBI's ability to internally convert ornithine to proline supported its own Stickland metabolism, depriving the pathogen of this nutrient source, while potentially increasing its ability to compete with *C. difficile*. This example highlights the importance of defining signals of efficacy for microbiota-derived products at the level of the target molecules, microbial genes, and effects on other microbes and the host.

CBI further affected multiple aspects of *C. difficile* physiology to reduce the pathogen's growth and toxin production, factors that persisted in the absence of *C. difficile's* CodY and CcpA PaLoc repressors (*40, 43*). As an active Stickland fermenter, CBI depleted amine-containing carbon sources and simple carbohydrates preferred by *C. difficile*, leaving sugar alcohols and more complex carbohydrates available. In response, *C.*

difficile adjusted its metabolism for these carbon sources and for hypoxanthines enriched in CBI-monocolonization. Notably, *C. difficile's* protein translation machinery was significantly repressed *in vivo* with CBI-co-colonization, as were cellular lytic systems including diffocins, sporulation, cell-wall turnover enzymes, and oxidative stress pathways (Figure 6).

In vivo studies also illustrated pathogen and commensal population effects over the course of infection. The focal nature of early gut damage suggests localized events that can rapidly spread to alter host, pathogen and commensal behaviors. All three microbial species expressed oxidative stress or detoxification systems with the onset of symptomatic infection, effects indicative of the substantial luminal changes brought on by the host's inflammatory responses. The up-regulation of sporulation and oxidative stress responses by both *C. difficile* and CSAR when co-colonized, including the spore coat proteins superoxide dismutase (*sodA*), and manganese catalase (*cotG*), illustrated responses that in the confined space of the gut lumen may benefit vegetative cell populations of the same and other species by detoxifying host-produced ROS.

Interestingly, CBI is a microaerophilic species, able to tolerate 8% O2, concentrations at which CSAR and *C. difficile* cannot survive (*44*). By 20h of infection, CBI's Stickland gene expression was down-regulated. However, by 24h of infection the commensal adjusted its metabolism, up-regulating pathways for ethanolamine and polyamine utilization, and fermentation of arginine to ornithine and proline. Two weeks after acute infection CBI-co-colonized mice demonstrated intact gut epithelium and reduced toxin levels (Figs. 1F, I).

Interventional studies in antibiotic-treated conventional mice illustrated CBI's efficacy as an oral bacteriotherapeutic when administered *after* the onset of symptomatic infection. The single dose of clindamycin enriched multiple fermentable amino acid and carbohydrate sources, sources that were also enriched in GF and CSAR-monocolonized mice prior to *C. difficile's* introduction, supporting relevance of findings from germfree infection studies. These findings support a broader systems-level view for combinations of metabolizable carbon sources that create nutrient states conducive to *C. difficile* colonization and rapid growth, particularly given the pathogen's diverse carbon source metabolism and responses that enable adaption to different gut environments.

As in CBI-co-colonized mice, therapeutic administration of CBI to conventional mice reduced pathogen biomass, acute toxin levels, and prevented lethal infection. CBI-administration depleted additional fermentable cabon sources, which may have occurred through direct and indirect interactions between CBI and the

recovering microbiota. CBI administration also improved recovery of host sphingosines and ethanolamide endocannabinoids that were depleted with clindamycin treatment. While these compounds may support the growth and metabolism of ethanolamine and lipid-metabolizing commensal species, effects of such changes on host physiology and inflammatory responses warrant further investigation.

In vivo, colonic stores of amino acids and carbohydrates originate from un-absorbed dietary, microbial or host-produced sources (*45*). Mucins, in particular, are rich in host-produced carbohydrates, amino acids including threonine, which was consumed by all three species, and the primary Stickland acceptor amino acids proline, glycine and leucine (*46*). While proline and glycine are consumed in the reductive Stickland pathways, leucine can be consumed in either the oxidative or reductive reactions. In combination, the Stickland acceptor amino acids can enable rapid pathogen growth (*47*), with increased risks for population crashes and induction of stress responses that can promote abrupt spikes in toxin release.

Stickland fermention is a hallmark of the metabolism of Cluster XI *Clostridia*, and occurs in other *Clostridial* clusters, notably *Clostridium scindens* (Cluster XIVa) which posseses machinery for the proline and glycine reductases but not for the reductive leucine pathway (Fig. S6). While conversion of pro-germination primary bile acids to germination-inhibitory secondary bile acids by *C. scindens* and other species has been hypothesized to mediate *in vivo* protection against *C. difficile* (*48, 49*), we show more fundamental capacity of commensal species, singly or in aggregate, to rapidly change the gut nutrient environment and resulting host responses to direct *C. difficile's* growth, cellular metabolism, and virulence. Notably, the CBI and CSAR strains monocolonized in mice did not demonstrate 7α-hydroxysterol-dehydrogenase activity in the bile acid metabolomic signatures (Supplemental Text), further emphasizing their modulation of disease outcomes independently of microbial bile salt transformations.

Stickland-fermenting species represent <1% of the human gut microbiota. Our findings highlight the importance of these low-abundance members upon growth-promoting nutrients for *C. difficile,* and identify conditions that could be created by these and other species to modulate *C. difficile's* virulence. These conditions act in concert with the host's digestive functioning, immune status, and other co-morbid conditions (*50*). Host and commensal effects may also explain why *C. difficile* genetic polymorphisms and effects identified *in vitro* do

not necessarily reflect behaviors seen *in vivo.* Armed with refined mechanistic knowledge, findings establish a robust framework in which to develop therapeutics with targeted efficacy and improved safety for this disease.

Acknowledgments: We thank Andrea Dubois, Cameron Friedman, Vladimir Yeliseyev, Qing Liu and Rebecca Krinzman for technical support, Teri Bowman for tissue sectioning, and Peter Sewell for graphic design support. RNA sequencing was performed by the Harvard Medical School Biopolymers Core Facility. Partners Healthcare's Enterprise Research Information Support (ERIS) provided support of the Massachusetts Host-Microbiome Center's high performance computing resources. We would also like to thank Jessica Allegretti, Laurent Bouillaut, Laurie Comstock and Aimee Shen for critical reading of the manuscript and helpful comments. This work was supported by the BWH Precision Medicine Institute, Harvard Digestive Diseases Center grant P30 DK034854, and a capital grant from the Massachsuetts Life Sciences Center. BP is supported by T32 HL007627; JW receives salary support from the National Center of Biocomputing Information, and JP from the Institut Pasteur (Bourse ROUX).

Supplementary Materials

- Materials and Methods
- Tables S1-S4
- Figures S1-S11
- Supplementary Text
- Supplemental Data Files 1-10

Materials and Methods

Bacterial strains and culture conditions

Table S1 shows the bacterial strains and their *in vitro* culture conditions. For quantitation of *C. difficile* and commensal biomass, mouse cecal contents were collected into pre-weighed Eppendorf tubes with 0.5mL of pre-

reduced PBS with 40mM cysteine (Sigma Chemical, St. Louis, MO) as a reducing agent. Tubes were weighed after adding material and transferred into a Coy anaerobic chamber (Coy Labs, Grass Lake, MI) at 37°C for serial dilutions with plating to selective *C. difficile* CHROMID agar (Biomérieux, Durham, NC) or Brucella agar (Becton Dickinson, Canaan, CT) for commensal quantitation. *C. difficile* colonies were counted at 48 hours of incubation and identified as large black colonies. For the ΔcodY ΔccpA double mutant, colonies were quantitated at 72 hours of incubation. Commensal colonies were counted after 24 hours of incubation. CSAR colonies were identified as small, round beta-hemolytic colonies. CBI were identified as opaque and larger round colonies. Representative colonies were species-confirmed using rapid ANA panels (Remel, Lenexa, KS). For studies in conventional mice, pre-infection and post-clindamycin fecal pellets showed no positive colonies on CHROMID agar.

C. difficile spore preparations and counts were defined by exposing pre-weighed material to 50% ethanol for 60 minutes followed by serial dilution and plating to *C. difficile* CHROMID agar, as described (*51*).

Vegetative cell biomass was calculated by subtracting the spore biomass from the total biomass and normalizing to the cecal mass. Data were evaluated in Prism 8.0 (GraphPad, San Diego, CA) for visualization and log-rank tests of significance among groups. A p value <0.05 was considered significant.

Construction of *C. difficile codY, ccpA* and double *codY ccpA* mutant strains

Table S2 indicates plasmid vectors and primer sequences used to generate gene-deleted mutants in ATCC43255. Mutants were created using a newly developed Allele-Coupled Exchange (ACE) vector, derived from pMTL-SC7215, a *codA*-based "pseudosuicide" plasmid that replicates in the cells at a rate lower than that of the host chromosome (*52*). The *codA* cassette was removed by inverse PCR and replaced with the RCd8-*CD2517.1* type I toxin-antitoxin module from *C. difficile* 630 using NEBuilder HiFi DNA Assembly (NEB), yielding pMSR0 (*53*). In this vector, the *CD2517.1* toxin gene was placed under control of the P_{tet} inducible promoter and the Rcd8 antitoxin was expressed from its own promoter. For deletions, allelic exchange cassettes were designed to have approximately 900 bp of homology to the chromosomal sequence in both up- and downstream locations of the sequence to be altered. The homology arms were amplified by PCR from *C. difficile* strain

ATCC43255 genomic DNA (Table S1) and purified PCR products were cloned into the PmeI site of pMSR0 using NEBuilder's HiFi DNA Assembly.

pMSR0-derived plasmids were transformed into *E. coli* strain NEB10β and inserts verified by sequencing. Plasmids were then transformed into *E. coli* HB101 (RP4) and transferred by conjugation into *C. difficile* ATCC43255 after a brief period of heat shock (*54*). The procedure for allelic exchange follows that used for the *codA*-mediated allelic exchange method (*52*), except counter-selection is based on inducible expression of the *CD2517.1* toxin gene. Transconjugants were selected on BHI supplemented with cycloserine (250 µg/ml), cefoxitin (25 µg/ml) and thiamphenicol (15 µg/ml), and then restreaked onto BHI agar with thiamphenicol (15 µg/ml). After 24h, faster-growing single-crossover integrants formed visibly larger colonies. Individual colonies were re-streaked to BHI + thiamphenicol (15 µg/ml) to ensure purity of the single crossover integrant. Purified colonies were then re-streaked to BHI plates containing 100 ng/ml of the non-antibiotic analog anhydrotetracycline (ATc) to select for cells in which the plasmid had excised. In the presence of ATc, cells in which the plasmid is still present will produce CD2517.1 at toxic levels and will not form colonies. Clones were then confirmed by PCR for the expected deletion.

Mouse Studies

All animal studies were conducted under an approved institutional IACUC protocol. Defined-colonization experiments were conducted in negative pressure BL-2 gnotobiotic isolators (Class Biologically Clean, Madison, WI). Conventional studies were conducted in OptiMice containment cages (Animal Care Systems, Centennial, CO). Mice were singly housed for all studies.

Gnotobiotic Mouse Colonization and Infection Studies

One week prior to infection with *C. difficile* equal ratios of 6-7 week old male and female gnotobiotic mice were gavaged with $1x10^8$ CFU of *C. bifermentans* (CBI), *C. sardiniense* (CSAR), or sterile vehicle control, and allowed to colonize for 7 days prior to challenge with $1x10^3$ of wild-type or mutant *C. difficile* spores. Fecal pellets from

mice were cultured prior to infection to confirm association with the defined species, or maintenance of the GF state. Progression of disease was assessed via body condition scoring (*55*) and body mass measurements taken by ethylene-oxide sterilized, battery powered OHAUS scales (Thermo-Fisher, Waltham, MA). Mice were sacrificed at a BCS of 2-, or at defined timepoints at 7 days of commensal monocolonization or GF controls, and at 20, 24h or 14 days post-*C. difficile* challenge. For *C. difficile* mutant infection studies, timepoints at 16h and 24h post-challenge were collected. Cecal contents were collected for functional studies. The GI tract and internal organs were fixed in zinc-buffered formalin (Z-FIX, Thermo-Fisher, Waltham, MA) for histopathologic assessment.

Conventional Mouse Infection Studies

5-week old conventional mice (Taconic Farms, Inc., Taconic, NY) were singly housed and acclimated for a week prior to treatment with USP-grade clindamycin phosphate (10mg/kg; Sigma Chemical, St. Louis, MO) via intraperitoneal (IP) injection. 24 hours post-clindamycin treatment, mice were challenged with $1x10^3$ wild-type *C. difficile* spores via oral gavage and treated with $1x10^8$ CFU of *C. bifermentans* (CBI) or vehicle control at 12h post *C. difficile* challenge, the earliest point of symptomatic diarrhea in conventional mice. Progression of disease was assessed via BCS and body mass measurements. Survival studies were followed to 14 days post *C. difficile* challenge. For *C. difficile* biomass, toxin B levels and cecal metabolomic studies, 12 mice per group were also sacrificed and cecal contents collected at pre-clindamycin treatment, post-clindamycin treatment just prior to *C. difficile* challenge, 30 hours *post C. difficile* challenge, and at 14 days following control or CBI treatment.

Histopathologic Analyses

Formalin-fixed segments of small bowel, cecum and colon from GF or specifically-associated mice were paraffin embedded and 5um sections cut for staining with hematoxylin and eosin (H&E; Thermo-Fisher, Waltham, MA) as described (*56*). Stained slides were visualized under a Nikon Eclipse E600 microscope (Nikon, Melville, NY)

for assessments of toxin-mediated epithelial damage, as evidenced by cellular stranding and vacuolation, and to assess the natures of Inflammatory infiltrates, mucosal erosions, and tissue edema.

Toxin B ELISA

Cecal toxin B levels were quantified as described (*57*). Briefly, microtiter plates were coated with 10ug/mL of anti-TcdB capture antibody (BBI solutions, Madison, WI). Supernatants of spun cecal contents and standard curve controls of toxin B (Campbell, CA) were assayed in triplicate. After incubation and washing a paired anti-toxin B biotinylated antibody (mouse-anti-*Clostridium difficile* TcdB; (BBI solutions, Madison, WI) followed by high Sensitivity Streptavidin-HRP conjugate (Thermo-Fisher, Waltham, MA), and signal detected with TMB substrate (Thermo-Fisher, Waltham, MA) at 450nm using a BioTek Synergy H1 plate reader (Biotek Instruments Inc, Winoski, VT). Values were analyzed in Prism 8.0 (GraphPad, San Diego, CA) to calculate ug of toxin B/gram of cecal contents. Significant differences among groups were evaluated by non-parametric Kruskal-Wallis ANOVA and Dunn's post-test. A p value ≤ 0.05 was considered significant.

Effects of Commensal Colonization on Toxin Function

The Quidel *C. difficile* cell culture functional toxin assay (*58*) was used to evaluate if commensal colonization altered the functional toxicity of *C. difficile* toxin. Cecal contents were collected from germfree mice or from mice monocolonized for 7 days with *C. bifermentans, or C. sardiniense*. 100uL of purified toxin B control solution (Quidel Inc., San Diego, CA) was added to 1 gram of cecal contents and incubated for 30 minutes prior to making 1:10 to 1:500 serial dilutions in the Quidel-provided dilution buffer and adding materials to confluent cultures of human MRC-5 fibroblasts. Fibroblast cells were incubated at 37°C for 48 hours and checked daily by compound microscope for signs of cytopathic effect (CPE) indicated by balling up of cells and loss of adhesion. Additional control samples included cecal contents incubated with toxin B for 30 minutes followed by addition of neutralizing antibody to confirm specificity of CPE by toxin B. Cells where CPE occurred in the presence of toxin B, but not with cecal contents alone or with neutralizing antibody were called positive. All conditions were repeated in triplicate. The highest dilution at which CPE occurred was identified for each condition.

Western blot for Toxin B Integrity

Cecal supernatants from mice at 20h of infection extracted and subjected to SDS-PAGE and transfer to PVDF membrane (PerkinElmer, Waltham, MA) as described (*59*). Toxin B was detected with a sheep primary antibody (R&D Systems, Minneapolis MN), diluted 1:1000 in 5% nonfat dry milk blotting buffer (25mM Tris, pH 7.4, 0.15M NaCl, 0.1% Tween 20), with bound antibody detected with a donkey anti sheep HRP-conjugated secondary antibody, diluted 1:1000 in 5% nonfat dry milk blotting buffer (25mM Tris, pH 7.4, 0.15M NaCl, 0.1% Tween 20) (R&D Systems, Minneapolis MN), and detected by chemiluminescence using the SuperSignal West Pico Plus Western Blotting Substrate (part# 34577; Thermo-Scientific, Waltham, MA).

Metabolomic studies

For GF colonization studies cecal contents from 8 mice per group across 2 experimental replicates were harvested from GF mice at baseline, after 7 days of monocolonization with CBI or CSAR, and at 20h post-infection with *C. difficile* alone or with each commensal (6 groups, 48 mice total). For conventional studies, cecal contents were collected from 12 mice per group prior to clindamycin treatment, 24h post-clindamycin treatment, and at 30h post *C. difficile* challenge, at the height of symptomatic infection. Materials were snap frozen into pre-weighed tubes and weighed to determine mass of cecal contents. Global metabolomic screen of samples was performed by Metabolon (Raleigh, NC) with sample extraction and MALDI-TOF analyses as described (*60, 61*). Results were obtained as Original Scale mass spectrometry counts.

Quantification of Short Chain Fatty Acids (SCFA)

Volatile short chain fatty acids from specifically-associated mice were quantified as described (*26*). In brief, acidified internal standards with 100 µL of ethyl ether anhydrous or boron trifluoride-methanol was added to 100ul of supernatant from homogenized cecal contents. Chromatographic analyses were carried out on an Agilent 7890B system with flame ionization detector (FID). Chromatogram and data integration was carried out using the OpenLab ChemStation software (Agilent Technologies, Santa Clara, CA). SCFA in samples were identified by comparing their specific retention times relative to the retention time in the standard mix.

Concentrations were determined and expressed as mM of each SCFA per gram of sample for the raw cecal/fecal material. The Agilent platform cannot discriminate between isovalerate and 2-methylbutyrate and thus reports these compounds out as a single peak and interpolated value.

Carbon Source Enrichment Analyses

A variation of pathway enrichment analysis (*62*) was used to evaluate carbon source availability and consumption *in vivo*. Curated carbon source groups, optimized to reflect carbon source metabolism of gut commensal species, was developed with review of primarily literature regarding anaerobic metabolism of carbohydrate, amino acid and other amine-containing compounds, lipids, aromatic compounds, purines and pyrimidines, vitamins, micronutrients and other input sources for microbial metabolism and growth. Additional sources of reviewed information included published maps of *C. difficile's* biochemical pathways (*63, 64*) and BioCyc and MetaCyc content for *C. difficile* strain CD630 (*62*). A carbon source group required a minimum of 6 biochemicals for evaluation. For studies in GF mice, 506 biochemicals, of 787 identified by the Metabolon panel, 64.3% of the dataset, were curated into carbon source groups (SDF 1.1-1.2). For studies in conventional mice, 667 biochemicals of 858, 77.8% of the dataset, were curated into carbon source groups (SDF 9.1-9.2).

Mass spectrometry datasets were filtered to remove biochemicals with values <50,000 counts across all sample (<3% of biochemicals). Remaining zero-value data points were assigned a value of 25,000 to support calculation of Log2 fold-change between comparisons. Datasets were Log2 transformed for significance testing of each biochemical by Welch's T test and Benjamini-Hochberg multi-hypothesis correction (*65, 66*). Thresholds for enrichment used a Log2 fold-change of ≥0.32192809 (1.25X), and a Log2 fold-change ≤ -0.32192809 (-1.25X) for depletion, and per-biochemical adjusted p value ≤0.05. Biochemicals in pairwise comparisons were ranked by adjusted p value and up to the top 40% of significantly changing biochemicals were used in analyses.

The number of enriched and depleted biochemicals per carbon source group, and total number of enriched and depleted biochemicals in datasets were calculated. Carbon source groups with ≥4 enriched or ≥4 depleted biochemicals underwent hypothesis testing by hypergeometric test, followed by Benjamini-Hochberg multi-hypothesis correction (*65*). An adjusted p value ≤0.05 for enriched or depleted carbon source groups was considered significant. Significantly enriched or depleted groups were plotted using the Python library Matplotlib

(*67*). Results for biochemicals within enriched groups were plotted in OriginLab (OriginLab, Wellesley Hills, MA) using the 3D XYY function, or with the Metaboanalyst 4.0 visualization tools (*68*).

Global Metabolomic Pathway Enrichment Analyses

Enrichment analyses were performed as described using the Metabolon and KEGG-designated sub-pathway content for identified biochemicals (SDF 1.3, 9.3). Analyses of germfree and monocolonized mice used 747 of 787 of identified biochemicals (95% of the dataset; SDF 1.3). Analyses of conventional mice used 842 of 858 identified metabolites (98.2% of the dataset; SDF 9.3). Metabolites not included in pathway analyses had <6 biochemicals in the sub-pathway defined groups.

Stickland Aromatic Metabolite Clustering

Stickland aromatic amino acid and histidine metabolites with known specificity for *C. difficile* or CBI (*11, 69*) were clustered by mouse sample using the Metaboanalyst 4.0 clustering tools and Pearson's correlation matrices (*68*). Similarities among samples were evaluated by amova (*70*).

Carbon source group clustering among pre-*C. difficile* conditions

Biochemicals present in both the specifically-colonized and conventional mouse datasets were combined to evaluate similarities among enriched carbon source groups in germfree, CBI- or CSAR-monocolonized mice, and the pre-clindamycin and post-clindamycin metabolomic profiles in conventional mice. The biochemicals in common carbon source groups enriched in both specifically-colonized and conventional mice were subjected to principal components analysis using the Metaboanalyst 4.0 PCA tool (*68*). The Pearson's distances among samples were evaluated by amova using mothur v.1.43.0 (*70*) to evaluate significant similarities among groups.

RNA extraction, prokaryotic mRNA enrichment and library preparation

RNA was extracted from 15-20mg of flash frozen cecal contents (n=6 mice per group) using the Zymo Direct-zol RNA purification kit (R2081; Zymo, Irvine, CA). The quality of extracted RNA was assessed using an Agilent 2100 Bioanalyzer (Agilent Technologies, Lexington, MA) and samples with RNA Integrity Number (RIN) >= 8.0 were processed through Ribo-Zero Gold rRNA removal kit (MRZH116; Illumina, San Diego, CA) or NEBNext

bacterial and rRNA Depletion Kit to deplete prokaryotic and eukaryotic rRNAs, and eukaryotic poly-A mRNAs (New England Biolabs, Ipswich, MA). The transcriptome sequencing libraries were constructed using the Illumina TruSeq mRNA Library Prep kit (20020594, 20020493; Illumina, San Diego, CA) or NEBNext Ultra II Directional RNA library prep kit (New England Biochemical, Ipswich, MA), per the manufacturer's specifications. Library sizes were checked using a Bioanalyzer DNA High Sensitivity chip and TapeStation and quantified using Qubit dsDNA HS Assay Kit (Q32854; Thermo-Fisher, Waltham, MA). For sequencing runs, 12 libraries were pooled and sequenced on an Illumina Nextseq500 (Illumina, San Diego, CA) in paired-end 150 (PE150) nucleotide runs.

Transcriptome Data Processing

Reference bacterial and mouse genomes for *C. difficile* ATCC43255 (NZ_CM000604.1) and *C. bifermentans* ATCC638 (NZ_AVNC01000001.1) were obtained from the PATRIC Genome Annotation service (*71*) and *Mus musculus* C57BL6/J (GCF_000001635.26) from the NCBI host genome reference consortium to map reads. A genome for CSAR was generated using the methods as described in Nudel, et al (*72*) by Illumina MiSeq and was annotated in PATRIC (*73*).

Paired-end reads were quality filtered and trimmed then mapped to mouse and microbial genomes using Bowtie2 (*74*) using strict requirements for read orientation. The "--no-mixed" and "--no-discordant" flags were used to ensure that paired reads aligned to the same section of the genome in the expected orientation, respectively. Read pairs with a mapping quality <10, a measure of alignment uniqueness, were filtered. Reads aligning to >1 genome were flagged for subsequent analysis to identify potential sites of homology among genomes.

Mapped reads were assigned to gene features using HTSeq (*75*) with flags "--nonunique all" to allow reads mapping to multiple features to be called to account for polycistronic RNAs, and "-a 10" to set the minimum mapping quality score at 10, a measure of alignment uniqueness. The identity of unaligned reads was analyzed with Kraken2 (*76*) to confirm association of mice with the expected species. Supplemental Table 3 shows the total and average read counts mapped to *C. difficile*, CSAR, CBI, or mouse across experimental conditions and replicates.

HTSeq results from each experimental replicate were binned by species and formatted for DESeq2 analyses (*77*). Gene features where no set of experimental replicates averaged more than 10 reads per replicate were filtered from further analysis (<3% of genes). A widely used DESeq2 analysis template was modified for differential expression analysis (https://gist.github.com/stephenturner/f60c1934405c127f09a6). Read data from all experimental replicates of a given organism were included for pairwise DESeq2 analyses to insure the same adjusted read counts and estimates of dispersion across pairwise comparisons. Volcano plots showing the log2 fold change and adjusted p value for all analyzed genes, and Pearson's correlation matricies for each microbial transcriptome are shown in Figures S9-S11.

Transcriptome Pathway Enrichment Analyses

Table S4 shows the number genes and percent of gene features mapped into pathway categories for each microbe. For *C. difficile,* mappings leveraged multiple previously published gene-level and pathway annotations for CD630 (*64, 78, 79*) and the bacterial-based Riley schema to define microbial pathways and super-pathways (*80*), with addition of pathways such as "Mucin Degradation" to describe anaerobe-host categories, or ones that were missing or partially annotated in public resources. An operon map of *C. difficile* genes was created from the BioCyc content for the CD630 strain (*62*). Genes present in ATCC43255, but not CD630, were treated as single-cistron operons (SDF 3.1-3.2). PATRIC and PROKKA (*81*) annotation of the CSAR and CBI genomes were used to develop pathway maps for these species. Gene features in the commensals were also subjected to BLAST against the CD630 reference genome to provide additional annotation information. The annotated microbial gene features are shown in SDF 3.2-3.4 for *C. difficile, C. sardiniense* and *C. bifermentans,* respectively.

A minimum of 8 genes across at least 2 putative operon structures were required to define a pathway category. Thresholds for gene enrichment or depletion were set at +/-1.5X fold-change (Log2 fold-change of +/-0.584962501) and with a DESeq2 per-gene adjusted p value ≤0.05. Up to the top 40% of significantly changing genes, ranked by the per-gene adjusted p value, were analyzed in each pairwise comparison. Pathways with a minimum of 5 enriched or of 5 depleted genes underwent hypothesis testing by hypergeometric test. Multi-hypothesis adjusted p values were calculated using the Benjamini-Hochberg method (*65*). Pathways with an

adjusted p value ≤0.05 were considered significant. Enriched pathways were plotted using Python library Matplotlib (*67*). Heatmaps of all genes in enriched or depleted pathway categories were visualized using the Metaboanalyst 4.0 microbiome tools (*68*), with hierarchical gene-level clustering by Pearson similarity and minimum-distance linkage.

Genomic DNA extraction and qPCR

Genomic DNA was extracted from cecal contents using the Zymo Quick-DNA Fecal/Soil Microbe Miniprep Kit (kit# 11-322; Zymo, Irvine, CA) and qPCR was performed using Taqman primers and probes specific for *C. bifermentans, C. sardiniense* and *C. difficile* with the conditions as described (*6, 51*) on a QuantStudio 12K Flex Real time PCR system (Applied Biosystems, Beverly, MA). Samples were run in triplicate and compared against standard curves of known biomass of each organism spiked into germfree cecal contents and then extracted to provide normalized CFU counts per gram of cecal contents.

References

1. K. Aktories, Bacterial protein toxins that modify host regulatory GTPases. *Nat Rev Microbiol* **9**, 487-498 (2011).
2. J. R. Allegretti *et al.*, Clinical Predictors of Recurrence After Primary Clostridioides difficile Infection: A Prospective Cohort Study. *Dig Dis Sci*, (2019).
3. J. A. K. McDonald *et al.*, Inhibiting Growth of Clostridioides difficile by Restoring Valerate, Produced by the Intestinal Microbiota. *Gastroenterology* **155**, 1495-1507 e1415 (2018).
4. R. C. Vemuri, R. Gundamaraju, T. Shinde, R. Eri, Therapeutic interventions for gut dysbiosis and related disorders in the elderly: antibiotics, probiotics or faecal microbiota transplantation? *Beneficial microbes* **8**, 179-192 (2017).
5. E. M. Giles, G. L. D'Adamo, S. C. Forster, The future of faecal transplants. *Nat Rev Microbiol*, (2019).
6. A. Abdel-Gadir *et al.*, Microbiota therapy acts via a regulatory T cell MyD88/RORgammat pathway to suppress food allergy. *Nat Med* **25**, 1164-1174 (2019).
7. W. Zhu *et al.*, Gut Microbial Metabolite TMAO Enhances Platelet Hyperreactivity and Thrombosis Risk. *Cell* **165**, 111-124 (2016).
8. L. Bouillaut, T. Dubois, A. L. Sonenshein, B. Dupuy, Integration of metabolism and virulence in Clostridium difficile. *Res Microbiol* **166**, 375-383 (2015).
9. M. Monot *et al.*, Clostridium difficile: New Insights into the Evolution of the Pathogenicity Locus. *Sci Rep* **5**, 15023 (2015).
10. C. R. Denise Mehner-Breitfeld, Thomas Riedel, Ingo Just, Ralf Gerhard, Jörg Overmann, Thomas Brüser, Evidence for an Adaptation of a Phage-Derived Holin/Endolysin System to Toxin Transport in Clostridioides difficile. *Frontiers in microbiology* **9**, 1664-1302X (2018).
11. M. Neumann-Schaal, D. Jahn, K. Schmidt-Hohagen, Metabolism the Difficile Way: The Key to the Success of the Pathogen Clostridioides difficile. *Frontiers in microbiology* **10**, 219 (2019).
12. L. Bouillaut *et al.*, Role of the global regulator Rex in control of NAD(+) -regeneration in Clostridioides (Clostridium) difficile. *Molecular microbiology* **111**, 1671-1688 (2019).
13. T. Dubois *et al.*, Control of Clostridium difficile Physiopathology in Response to Cysteine Availability. *Infection and immunity* **84**, 2389-2405 (2016).
14. K. L. Nawrocki, D. Wetzel, J. B. Jones, E. C. Woods, S. M. McBride, Ethanolamine is a valuable nutrient source that impacts Clostridium difficile pathogenesis. *Environmental microbiology*, (2018).
15. I. Martin-Verstraete, J. Peltier, B. Dupuy, The Regulatory Networks That Control Clostridium difficile Toxin Synthesis. *Toxins (Basel)* **8**, (2016).
16. B. M. Walter *et al.*, The LexA regulated genes of the Clostridium difficile. *BMC microbiology* **14**, 88 (2014).
17. A. N. Edwards, R. Tamayo, S. M. McBride, A novel regulator controls Clostridium difficile sporulation, motility and toxin production. *Molecular microbiology* **100**, 954-971 (2016).
18. S. Karlsson, L. G. Burman, T. Akerlund, Induction of toxins in Clostridium difficile is associated with dramatic changes of its metabolism. *Microbiology (Reading, England)* **154**, 3430-3436 (2008).
19. J. A. Ferreyra *et al.*, Gut microbiota-produced succinate promotes C. difficile infection after antibiotic treatment or motility disturbance. *Cell Host Microbe* **16**, 770-777 (2014).
20. D. Gebhart *et al.*, A modified R-type bacteriocin specifically targeting Clostridium difficile prevents colonization of mice without affecting gut microbiota diversity. *MBio* **6**, (2015).
21. R. Govind, G. Vediyappan, R. D. Rolfe, B. Dupuy, J. A. Fralick, Bacteriophage-mediated toxin gene regulation in Clostridium difficile. *J Virol* **83**, 12037-12045 (2009).
22. T. H. Tam Dang, R. P. Fagan, N. F. Fairweather, E. W. Tate, Novel inhibitors of surface layer processing in Clostridium difficile. *Bioorganic & medicinal chemistry* **20**, 614-621 (2012).

23. I. El Meouche, J. Peltier, Toxin release mediated by the novel autolysin Cwp19 in Clostridium difficile. *Microbial cell (Graz, Austria)* **5**, 421-423 (2018).
24. N. Kint *et al.*, The alternative sigma factor sigma(B) plays a crucial role in adaptive strategies of Clostridium difficile during gut infection. *Environmental microbiology* **19**, 1933-1958 (2017).
25. M. Neumann-Schaal *et al.*, Tracking gene expression and oxidative damage of O2-stressed Clostridioides difficile by a multi-omics approach. *Anaerobe* **53**, 94-107 (2018).
26. L. Moore, Moore, WEC, *Anaerobe Lab Manual*. (VPI, Blacksburg, VA, ed. 4th, 1993).
27. N. van der Wielen, P. J. Moughan, M. Mensink, Amino Acid Absorption in the Large Intestine of Humans and Porcine Models. *J Nutr* **147**, 1493-1498 (2017).
28. C. M. Theriot *et al.*, Antibiotic-induced shifts in the mouse gut microbiome and metabolome increase susceptibility to Clostridium difficile infection. *Nat Commun* **5**, 3114 (2014).
29. O. W. Griffith, R. J. Bridges, A. Meister, Transport of gamma-glutamyl amino acids: role of glutathione and gamma-glutamyl transpeptidase. *Proceedings of the National Academy of Sciences of the United States of America* **76**, 6319-6322 (1979).
30. W. Bradshaw, Barker HA., Purification and properties of xanthine dehydrogenase from Clostridium cylindrosporum. *Journal of Biological Chemistry* **235**, 3620-3629 (1960).
31. G. D. Vogels, C. Van der Drift, Degradation of purines and pyrimidines by microorganisms. *Bacteriol Rev* **40**, 403-468 (1976).
32. J. Kim, D. Darley, T. Selmer, W. Buckel, Characterization of (R)-2-hydroxyisocaproate dehydrogenase and a family III coenzyme A transferase involved in reduction of L-leucine to isocaproate by Clostridium difficile. *Appl Environ Microbiol* **72**, 6062-6069 (2006).
33. J. A. Sorg, A. L. Sonenshein, Chenodeoxycholate is an inhibitor of Clostridium difficile spore germination. *Journal of bacteriology* **191**, 1115-1117 (2009).
34. M. B. Francis, C. A. Allen, J. A. Sorg, Muricholic acids inhibit Clostridium difficile spore germination and growth. *PloS one* **8**, e73653 (2013).
35. D. Bakonyi, W. Hummel, Cloning, expression, and biochemical characterization of a novel NADP(+)-dependent 7alpha-hydroxysteroid dehydrogenase from Clostridium difficile and its application for the oxidation of bile acids. *Enzyme Microb Technol* **99**, 16-24 (2017).
36. Y. Lee, J. Jo, H. Y. Chung, C. Pothoulakis, E. Im, Endocannabinoids in the gastrointestinal tract. *Am J Physiol Gastrointest Liver Physiol* **311**, G655-G666 (2016).
37. N. Fonknechten *et al.*, A conserved gene cluster rules anaerobic oxidative degradation of L-ornithine. *Journal of bacteriology* **191**, 3162-3167 (2009).
38. S. I. Patterson-Curtis, E. A. Johnson, Roles of arginine in growth of Clostridium botulinum Okra B. *Appl Environ Microbiol* **58**, 2334-2337 (1992).
39. T. Bosak, R. M. Losick, A. Pearson, A polycyclic terpenoid that alleviates oxidative stress. *Proceedings of the National Academy of Sciences of the United States of America* **105**, 6725-6729 (2008).
40. S. S. Dineen, S. M. McBride, A. L. Sonenshein, Integration of metabolism and virulence by Clostridium difficile CodY. *Journal of bacteriology* **192**, 5350-5362 (2010).
41. M. Bielaszewska *et al.*, Effects of antibiotics on Shiga toxin 2 production and bacteriophage induction by epidemic Escherichia coli O104:H4 strain. *Antimicrobial agents and chemotherapy* **56**, 3277-3282 (2012).
42. J. L. Fachi *et al.*, Butyrate Protects Mice from Clostridium difficile-Induced Colitis through an HIF-1-Dependent Mechanism. *Cell reports* **27**, 750-761 e757 (2019).
43. A. Antunes *et al.*, Global transcriptional control by glucose and carbon regulator CcpA in Clostridium difficile. *Nucleic Acids Res* **40**, 10701-10718 (2012).
44. K. M. Katarzyna Leja, Mariola Olkowicz, Wojciech Juzwa, Katarzyna Czaczyk, Clostridium bifermentans as an Aero-Tolerant Exponent of Strictly Anaerobe Genera. *Advances in Microbiology* **4**, 216-224 (2014).

45. R. Li *et al.*, Different dietary protein sources in low protein diets regulate colonic microbiota and barrier function in a piglet model. *Food Funct*, (2019).
46. A. Wesley *et al.*, Neutral and acidic species of human intestinal mucin. Evidence for different core peptides. *J Biol Chem* **260**, 7955-7959 (1985).
47. E. J. Battaglioli *et al.*, Clostridioides difficile uses amino acids associated with gut microbial dysbiosis in a subset of patients with diarrhea. *Science translational medicine* **10**, (2018).
48. J. D. Kang *et al.*, Bile Acid 7alpha-Dehydroxylating Gut Bacteria Secrete Antibiotics that Inhibit Clostridium difficile: Role of Secondary Bile Acids. *Cell Chem Biol* **26**, 27-34 e24 (2019).
49. S. Bhowmik *et al.*, Structure and functional characterization of a bile acid 7alpha dehydratase BaiE in secondary bile acid synthesis. *Proteins* **84**, 316-331 (2016).
50. K. Solomon *et al.*, Mortality in patients with Clostridium difficile infection correlates with host pro-inflammatory and humoral immune responses. *Journal of medical microbiology* **62**, 1453-1460 (2013).
51. V. Bucci *et al.*, MDSINE: Microbial Dynamical Systems INference Engine for microbiome time-series analyses. *Genome biology* **17**, 121 (2016).
52. S. T. Cartman, M. L. Kelly, D. Heeg, J. T. Heap, N. P. Minton, Precise manipulation of the *Clostridium difficile* chromosome reveals a lack of association between the *tcdC* genotype and toxin production. *Applied and environmental microbiology* **78**, 4683-4690 (2012).
53. A. Maikova *et al.*, Discovery of new type I toxin-antitoxin systems adjacent to CRISPR arrays in *Clostridium difficile*. *Nucleic acids research* **46**, 4733-4751 (2018).
54. J. A. Kirk, R. P. Fagan, Heat shock increases conjugation efficiency in Clostridium difficile. *Anaerobe* **42**, 1-5 (2016).
55. S. Fekete, I. Szakall, E. Andr ofszky, E. Kosa, I. Hullar, Body composition of mice of different body condition score and sex. *Acta Vet Hung* **44**, 399-410 (1996).
56. L. Bry, M. B. Brenner, Critical role of T cell-dependent serum antibody, but not the gut-associated lymphoid tissue, for surviving acute mucosal infection with Citrobacter rodentium, an attaching and effacing pathogen. *J Immunol* **172**, 433-441 (2004).
57. E. R. Zarandi, S. Mansouri, N. Nakhaee, F. Sarafzadeh, M. Moradi, Toxin production of Clostridium difficile in sub-MIC of vancomycin and clindamycin alone and in combination with ceftazidime. *Microbial pathogenesis* **107**, 249-253 (2017).
58. E. T. Beck *et al.*, Multicenter evaluation of the Quidel Lyra Direct C. difficile nucleic acid amplification assay. *Journal of clinical microbiology* **52**, 1998-2002 (2014).
59. B. P. Girinathan, J. Ou, B. Dupuy, R. Govind, Pleiotropic roles of Clostridium difficile sin locus. *PLoS Pathog* **14**, e1006940 (2018).
60. J. Ryals, K. Lawton, D. Stevens, M. Milburn, Metabolon, Inc. *Pharmacogenomics* **8**, 863-866 (2007).
61. J. R. Fletcher, S. Erwin, C. Lanzas, C. M. Theriot, Shifts in the Gut Metabolome and Clostridium difficile Transcriptome throughout Colonization and Infection in a Mouse Model. *mSphere* **3**, (2018).
62. A. Marco-Ramell *et al.*, Evaluation and comparison of bioinformatic tools for the enrichment analysis of metabolomics data. *BMC Bioinformatics* **19**, 1 (2018).
63. L. J. Pettit *et al.*, Functional genomics reveals that Clostridium difficile Spo0A coordinates sporulation, virulence and metabolism. *BMC genomics* **15**, 160 (2014).
64. C. Janoir *et al.*, Adaptive strategies and pathogenesis of Clostridium difficile from in vivo transcriptomics. *Infection and immunity* **81**, 3757-3769 (2013).
65. Y. H. Benjamini, Yosef Controlling the false discovery rate: a practical and powerful approach to multiple testing. *Journal of the Royal Statistical Society, Series B.* **57**, 289-300 (1995).

66. R. A. van den Berg, H. C. Hoefsloot, J. A. Westerhuis, A. K. Smilde, M. J. van der Werf, Centering, scaling, and transformations: improving the biological information content of metabolomics data. *BMC genomics* **7**, 142 (2006).
67. J. D. Hunter, Matplotlib: A 2D Graphics Environment. *Computing in Science & Engineering* **9**, 90-95 (2007).
68. J. Chong *et al.*, MetaboAnalyst 4.0: towards more transparent and integrative metabolomics analysis. *Nucleic Acids Res* **46**, W486-W494 (2018).
69. G. C. Mead, The amino acid-fermenting clostridia. *J Gen Microbiol* **67**, 47-56 (1971).
70. P. D. Schloss, Reintroducing mothur: 10 years later. *Appl Environ Microbiol*, (2019).
71. D. A. Antonopoulos *et al.*, PATRIC as a unique resource for studying antimicrobial resistance. *Brief Bioinform*, (2017).
72. K. Nudel *et al.*, Genomics of Corynebacterium striatum, an emerging multidrug-resistant pathogen of immunocompromised patients. *Clinical microbiology and infection : the official publication of the European Society of Clinical Microbiology and Infectious Diseases* **24**, 1016 e1017-1016 e1013 (2018).
73. A. R. Wattam *et al.*, PATRIC, the bacterial bioinformatics database and analysis resource. *Nucleic Acids Res* **42**, D581-591 (2014).
74. S. S. Langmead B, Fast gapped-read alignment with Bowtie 2. *Nat Methods* **9**, 357–359 (2012).
75. P. P. Anders S, Huber W, HTSeq—a Python framework to work with high-throughput sequencing data. *Bioinformatics* **31**, 166–169 (2015).
76. A. L. A. Neves, F. Li, B. Ghoshal, T. McAllister, L. L. Guan, Enhancing the Resolution of Rumen Microbial Classification from Metatranscriptomic Data Using Kraken and Mothur. *Frontiers in microbiology* **8**, 2445 (2017).
77. Y. Guo, C. I. Li, F. Ye, Y. Shyr, Evaluation of read count based RNAseq analysis methods. *BMC genomics* **14 Suppl 8**, S2 (2013).
78. M. Dembek *et al.*, High-throughput analysis of gene essentiality and sporulation in Clostridium difficile. *MBio* **6**, e02383 (2015).
79. J. D. Hofmann *et al.*, Metabolic Reprogramming of Clostridioides difficile During the Stationary Phase With the Induction of Toxin Production. *Frontiers in microbiology* **9**, 1970 (2018).
80. R. M, Functions of the gene products of Escherichia coli. *Microbiological reviews* **57**, 862–952 (1993).
81. T. Seemann, Prokka: rapid prokaryotic genome annotation. *Bioinformatics* **30**, 2068-2069 (2014).

Supplemental Tables

Table S1: Strains and Culture Conditions

Strain	Species	Source	Genotype	Broth Culture Conditions	Agar Media
ATCC 43255	*Clostridioides difficile*	ATCC	Wild-type	BHIS, 37°C, anaerobic	Cdiff CHROMID
DSM 638	*Clostridium bifermentans*	DSMZ	Wild-type	BHIS, 37°C, anaerobic	Brucella agar
DSM 599	*Clostridium sardiniense*	DSMZ	Wild-type	BHIS, 37°C, anaerobic	Brucella agar
NEB-10 beta	*Escherichia coli*	NEB	*Δ(ara-leu) 7697 araD139 fhuA ΔlacX74 galK16 galE15 e14- ϕ80dlacZΔM15 recA1 relA1 endA1 nupG rpsL* (Str^R) *rph spoT1 Δ(mrr-hsdRMS-mcrBC)*	Luria-Bertani (LB) Broth, 37°C, aerobic	LB agar
HB101 (RP4)	*Escherichia coli*	Sonenshein, AL	*supE44 aa14 galK2 lacY1* Δ(*gpt-proA*) 62 *rpsL20* (Str^R)*xyl-5 mtl-1 recA13* Δ(*mcrC-mrr*) *hsdS*$_B$ (r_B-m_B-) RP4 (Tra^+ IncP Ap^R Km^R Tc^R)	Luria-Bertani (LB) Broth, 37°C, aerobic	LB agar
ATCC 43255 ΔcodY	*Clostridioides difficile*	This study	ΔcodY	BHIS, 37°C, anaerobic	Cdiff CHROMID
ATCC 43255 ΔccpA	*Clostridioides difficile*	This study	ΔccpA	BHIS, 37°C, anaerobic	Cdiff CHROMID
ATCC 43255 ΔccpA ΔcodY	*Clostridioides difficile*	This study	ΔccpA ΔcodY	BHIS, 37°C, anaerobic	Cdiff CHROMID

ATCC: American Type Culture Collection (http://www.atcc.org)
DSMZ: German Collection of Microorganisms and Cell Cultures (https://bacdive.dsmz.de)
Δgene: Gene-deleted strains have full open reading frame deletion of the gene (see Materials and Methods)
BHIS: Brain Heart Infusion media supplemented with cysteine, hemin and vitamin K
CHROMID: Biomeriéux selective *C. difficile* CHROMID agar

Table S2. Plasmids and Oligonucleotides used in the present study.

Plasmids	Use	Source
pMTL-SC7215	*E. coli-C. difficile* shuttle vector for CodA-mediated allele exchange mutagenesis. Tm^R	(*52*)
pDIA6745	pRPF185 derivative carrying *Ptet-CD2517.1-RCd8-P* region	(*53*)
pMSR0	*E. coli-C. difficile* shuttle vector for toxin-mediated allele exchange mutagenesis. Tm^R	This study
pDIA6987	pMSR0 with construct for *codY* deletion	This study
pDIA6988	pMSR0 with construct for *ccpA* deletion	This study

Primer	Sequence (5' to 3')*	Use
JP416	GGATCCTCTAGAGTCGACG	5' pMTL-SC7215 linearization and codA removal
JP417	GTAATCATGGTCATATGGATACAG	3' pMTL-SC7215 linearization and codA removal
JP418	atccatatgaccatgattacCGAATTCTGCATCAAGCTAG	5' P_{tet}-*CD2517.1*-RCd8
JP609	acgtcgactctagaggatccGAAACTGAAAGAAATCAATGG	3' P_{tet}-*CD2517.1*-RCd8
JP675	ttttttgttaccctaagtttGCCAGACCAACATTTTAC	5' left arm Δ*codY*
JP676	tagattattgCACTTCACTTGCCATTTAATC	3' left arm Δ*codY*
JP677	aagtgaagtgCAATAATCTATATTTTATAGGTTTAGATTAGAAAAG	5' right arm Δ*codY*
JP678	agattatcaaaaaggagtttGTCTTGCTAGATAGTGTATAG	3' right arm Δ*codY*
JP679	GGTTGAAAAAGTGACTAAATCTG	5' screening Δ*codY*
JP680	CTACATATACTTATCAAATCCCCAC	3' screening Δ*codY*
JP681	ttttttgttaccctaagtttGGATATGGGTTATATTAATAGTATTG	5' left arm Δ*ccpA*
JP682	tttttctttcGCCTTTCATCTTCATCCTC	3' left arm Δ*ccpA*
JP683	gatgaaaggcGAAAGAAAAAAATAAAACTATTAAAATCAATC	5' right arm Δ*ccpA*
JP684	agattatcaaaaaggagtttCATTTGCATCAAACCTTAAATTG	3' right arm Δ*ccpA*
JP685	GATTCTTTGATGGTGAAGTAGG	5' screening Δ*ccpA*
JP686	CTTCTTCACTTAAATCCATGAG	3' screening Δ*ccpA*

*Lowercase bases indicate overlapping sequences

Table S3: Species-level Mapping of RNAseq Read Counts
SuppelementalTable3_ReadCounts.xlsx

Table S3 shows the total and percentage of reads passing quality filtering that were assigned to each microbe, or to mouse, in addition to ambiguous reads and reads not mapping to any genome.

Table S4: Microbial Gene Feature Coverage in Pathway Maps

Species	Strain	# Gene Features	# Mapped Features	% of Gene Features Mapped	# Hypothetical Genes	% Hypothetical Genes (Unmapped)
C. difficile	ATCC 43255	3195	2000	63%	530	17%
C. bifermentans	DSM 638	3247	1840	57%	1230	38%
C. sardiniense	DSM 599	3502	1992	57%	1053	35%

# of Gene Features: Number of features in RNAseq datasets after basemean filtering (Supplemental Methods)
# of Hypothetical Genes: Number of genes with "hypothetical protein" annotations from PROKKA and/or PATRIC

Supplemental Data Files

Supplemental Data Files	**Format**
SDF_01 - GF carbon source and KEGG sub-pathway maps; tabular enrichment results	Excel
SDF_02 – Heatmaps of biochemicals in enriched carbon source groups across *in vivo* conditions in germfree and specifically-associated mice	PDF
SDF_03 - *C. difficile*, CSAR and CBI gene content for transcriptome enrichment analyses	Excel
SDF_04 - Tabular results of *C. difficile* and commensal transcriptome enrichment analyses	Excel
SDF_05 - Heatmaps of gene expression in *C. difficile* significantly enriched pathways	PDF
SDF_06 - Heatmaps of gene expression in CSAR significantly enriched pathways	PDF
SDF_07 - Heatmaps of gene expression in CBI significantly enriched pathways	PDF
SDF_08 - Enriched and depleted genes not included in enrichment analyses	Excel
SDF_09 - CONV carbon source and KEGG sub-pathway maps; tabular enrichment results	Excel
SDF_10 – Biochemicals in enriched carbon source groups across *in vivo* conditions in conventional mice	PDF

Figures:

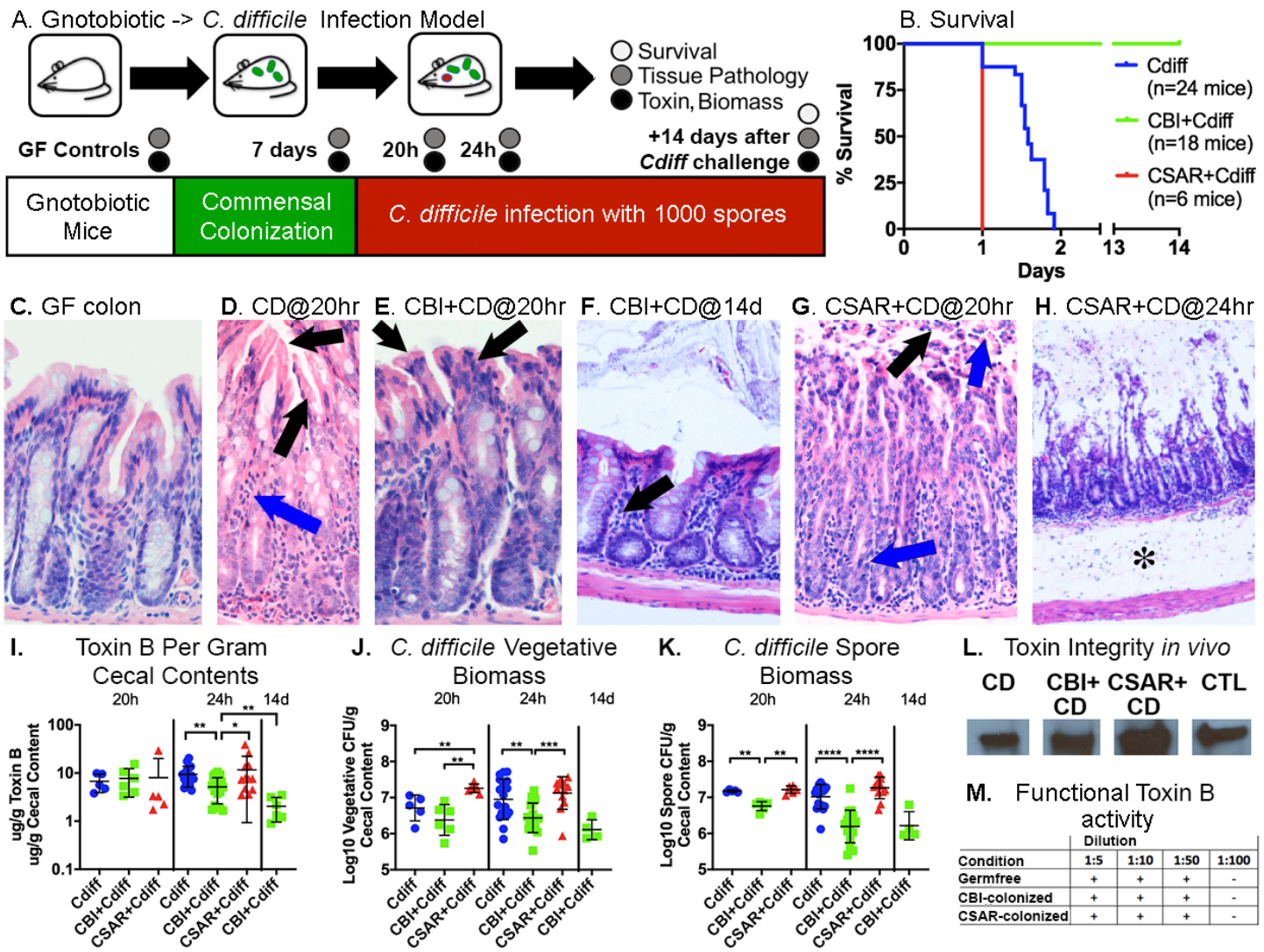

Condition	Dilution 1:5	1:10	1:50	1:100
Germfree	+	+	+	-
CBI-colonized	+	+	+	-
CSAR-colonized	+	+	+	-

Figure 1: CBI protects germfree mice from lethal *C. difficile* infection while CSAR promotes more severe disease. A: Experimental overview. **B**: Survival curves. **C-H:** Colonic H&E stains; C-E: 200X, F-G: 100X and H: 40X magnification. **C:** Normal germfree mucosa. **D:** *C. difficile*-infected mice at 20h, showing epithelial stranding and vacuolation (black arrows) and neutrophilic infiltrates (blue arrow). **E:** CBI-monocolonized mice at 20h of infection showing vacuolization of apical colonocytes (black arrows) but nominal inflammation. **F:** CBI+*C.* difficile-infected mice at 14d showing intact epithelium and lymphocytic infiltrates (black arrow). **G:** CSAR+*C. difficile*-infected mice at 20h showing surface epithelial loss (black arrow) and transmural neutrophilic infiltrates entering the lumen (blue arrows). **H:** CSAR-co-colonized mice at 24h of infection showing complete epithelial loss and severe submucosal edema (asterisk). **I:** Log10 ug/g of extracellular cecal Toxin B. Significance values by Mann-Whitney test: *0.01<p≤0.05; **0.001<p≤0.01; ***0.0001<p≤0.001; ****p≤0.0001. **J.** Log10 *C. difficile* vegetative CFU, and **K:** spore biomass/gram of cecal contents. **L.** Western blot of cecal contents showing intact toxin B in *C. difficile*-infected (CD), CBI or (CBI+CD), CSAR (CSAR+CD) co-colonized mice; CTL = control toxoid B. **M.** Effects of GF, CBI or CSAR-monocolonized cecal contents on toxin B function, no differences were noted.

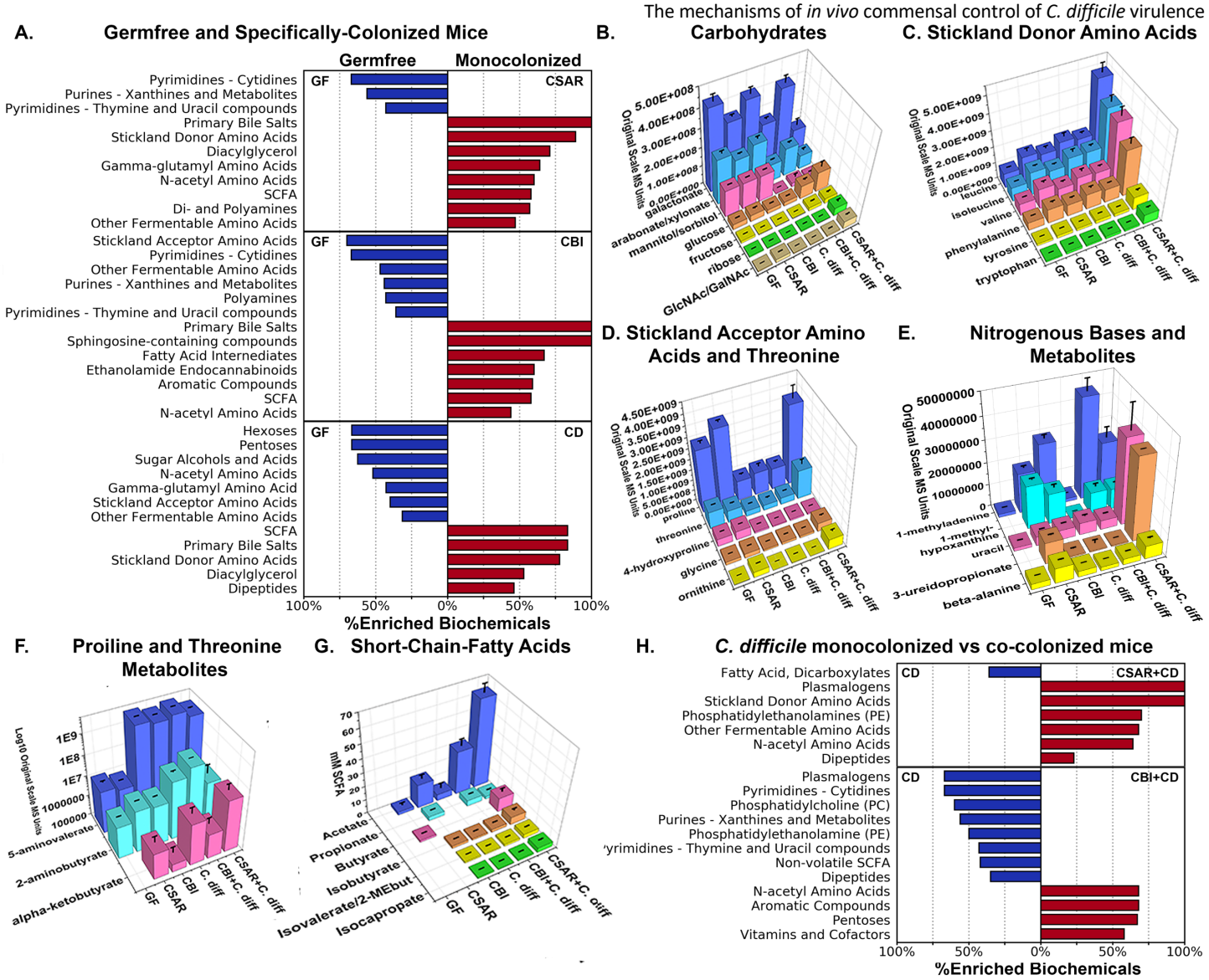

Figure 2: Cecal Carbon Source Enrichment Analyses in Colonized Mice. A: Significantly enriched carbon source groups in germfree (left-hand side) versus monocolonized mice (right-hand side). Groups with a Benjamini-Hochberg corrected p value≤0.05 are shown. Horizontal bars indicate the percent of biochemicals enriched in each carbon source group comparing germfree cecal contents with CSAR-monocolonized mice at 7 days (top), CBI-monocolonized for 7 days (middle), or *C. difficile*-monocolonized for 20h (bottom). **B-G:** Specifically-enriched compounds (Y-axis) across colonization states (X-axis). Z-axis shows original scale mass spectrometry counts. Error bars indicate standard error of the mean. Values for a given compound are comparable across experimental groups. **B.** Carbohydrates. **C:** Stickland donor amino acids. **D:** Stickland acceptor amino acids, proline-convertible compounds including hydroxyproline and ornithine, and threonine levels. **E:** Nitrogen base and uracil metabolites 3-ureidopropionate and beta-alanine. **F.** Proline and threonine metabolites, Z-axis shows Log10 original scale mass spectrometry counts. **G:** SCFA profiles. Z-axis shows mM of SCFA/gram of cecal contents. **H:** Significantly enriched carbon sources between *C. difficile*-monocolonized mice at 20h of infection (right-hand side) vs CSAR-monocolonized for 7 days + 20h of *C. difficile* infection (top) or CBI-monocolonized for 7 days + 20h of *C. difficile* infection (bottom).

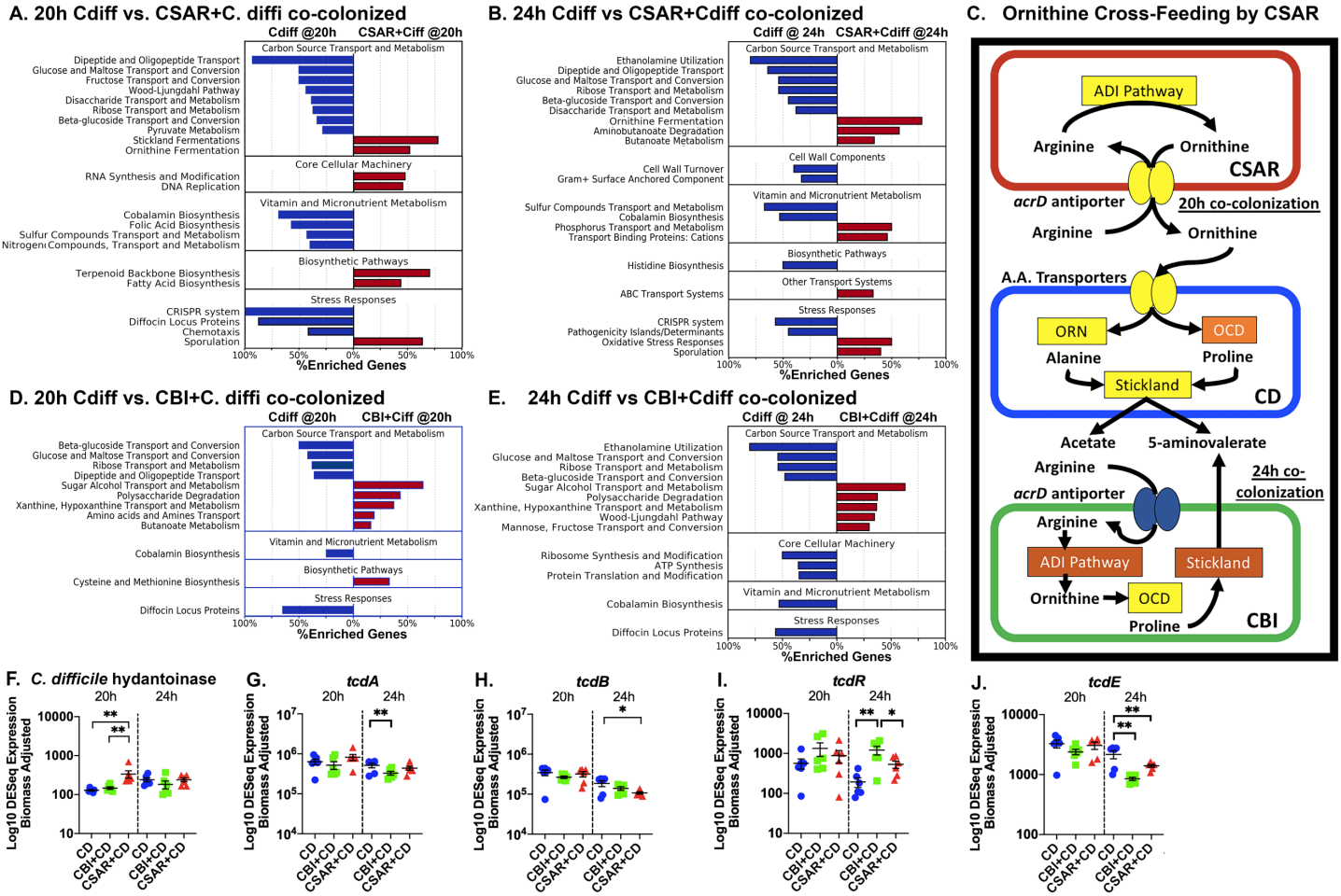

Figure 3: Pathway enrichment analyses of *in vivo C. difficile* transcriptomes. Horizontal bars indicate the percentage of genes within the pathway that were enriched in *C. difficile*-monocolonized mice (LH side) or in mice co-colonized with CSAR or CBI prior to *C. difficile* infection (RH side). Pathways with a Benjamini-Hochberg adjusted p value≤0.05 are shown. **A:** *C. difficile*-monocolonized mice at 20h of infection vs. CSAR and *C. difficile*-co-colonized mice. **B:** Same comparison as panel A but at 24h of infection. **C:** Cross-species pathways involved in ornithine cross-feeding of *C. difficile* by CSAR but not by CBI in co-colonized mice. **D.** Same comparison as in panel A at 20h of infection, comparing *C. difficile*-monocolonized with CBI-co-colonized mice. **E:** Same comparison as panel D. but at 24h of infection. **F:** Expression of *C. difficile* hydantoinase (geneID: UAB_RS0209810) that metabolizes uracil to 3-ureidoproprionate, showing up-regulation at 20h with CSAR-co-colonization (**p=0.0022). **Panels G-J:** DESeq-normalized reads for the PaLoc genes. X-axis indicates the colonization condition; Y-axis the Log10 DESeq normalized read counts that are normalized for biomass differences. Brackets indicate significant differences by Mann-Whitney log rank test. **G.** *tcdA* (**p=0.009), **H.** *tcdB* (*p=0.0142), **I.** *tcdR* (*p=0.0237; **p=0.002) and **J.** *tcdE* (**p=0.0022).

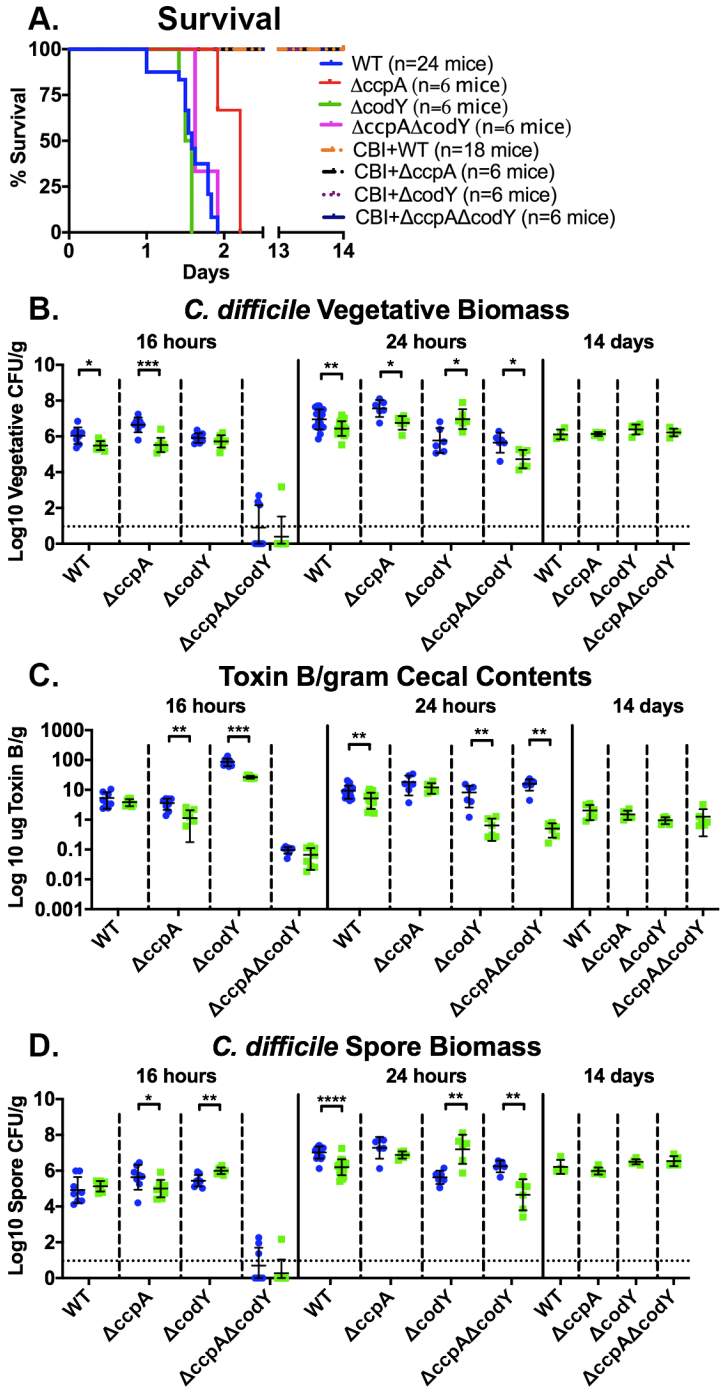

Figure 4: Infection with *ΔcodY*, *ΔccpA*, and *ΔcodY ΔccpA* mutant strains of *C. difficile*. A. Survival curves of GF and CBI-co-colonized mice infected with wild-type (WT) or mutant strains of *C. difficile*; n = at least 6 mice/group. The curves for all CBI-associated mice overlap. All CBI-associated mice were significantly different from mono-associated controls (p<0.0001). In monocolonized mice. *ΔcodY*-infected mice demonstrated more rapid decline than WT-infected mice (p=0.01), while in *ΔccpA*-infected mice, decline was delayed as compared to WT mice (p=0.0002). **B-D:** Cecal biomass and extracellular levels of toxin B. *C. difficile*-associated mice are shown in blue; Mice monocolonized with CBI and then infected with *C. difficile* are shown in green. Asterisks indicate significance values by Mann-Whitney log rank test: *0.01<p≤0.05; **0.001<p≤0.01; *** 0.0001<p≤0.001; ****p≤0.0001. **C.** Log10 of ug toxin B levels per gram of cecal contents. **D.** Log10 of *C. difficile* vegetative (**B.**) and spores (**C.**) in cecal contents at 16h, 24h, and at 14d in surviving CBI-co-colonized mice.

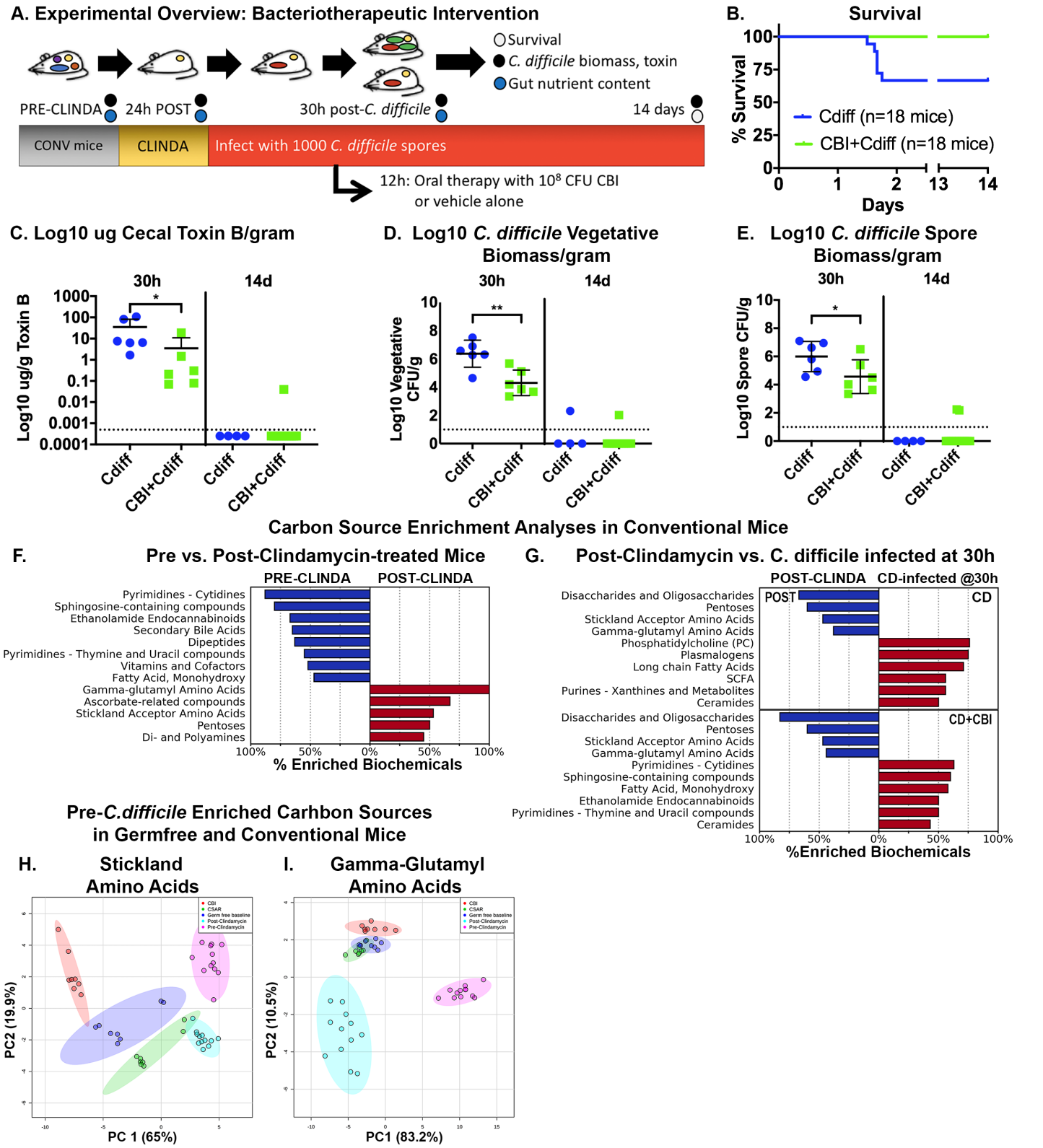

Figure 5: CBI protects *C. difficile*-infected conventional mice. A: Experimental overview. Samples for timed analyses (circles) were taken before and after clindamycin, at 30h post-infection (12h post-treatment), and at 14d in surviving mice. **B:** Survival curve; blue: *C. difficile*-infected and vehicle control treated; green: CBI-treated mice showed improved survival (p=0.0081). **C-E:** Cecal toxin and *C. difficile* biomass. Horizontal dotted line shows thresholds of detection. **C:** Log10 Toxin B per gram of cecal contents (*p=0.026). **D.** Log10 *C. difficile* vegetative (**p=0.0087) and **E:** spore biomass in cecal contents (p=*0.0411). **F:** Carbon source enrichment

analyses in mice pre- and post-clindamycin treatment showing enriched groups with a Benjamini-Hochberg corrected p value ≤0.05. **G:** Enriched carbon source groups between post-clindamycin treated and mice at 30 hours of infection with *C. difficile* (top) or with CBI-treatment (bottom). **H-I.** Principal components analysis (PCA) of carbon source groups enriched in pre-*C. difficile* conditions between germfree and conventional mice; Dark blue: germfree; Red: CBI-monocolonized; Green: CSAR-monocolonized; Pink: Pre-clindamycin-treated conventional mice; Light blue: Post-clindamycin-treated conventional mice. Shaded areas show 95% confidence region. **H.** Stickland Amino Acids, **I.** Gamma-glutamyl amino acids.

-

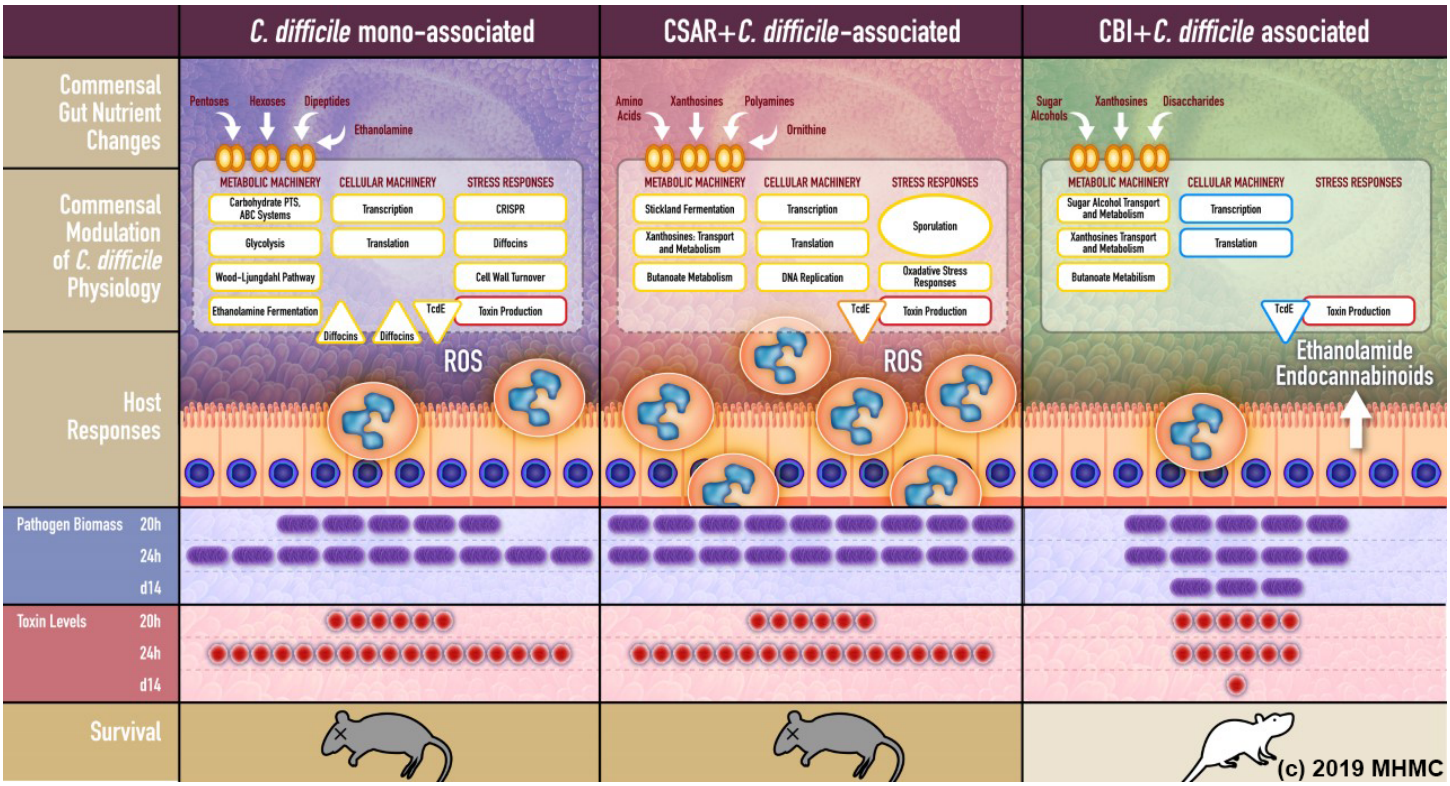

Figure 6: Mechanistic model of *in vivo* commensal control of *C. difficile* virulence. Schematic shows effects on *C. difficile* metabolism, cellular machinery and stress responses with *C. difficile*-monocolonization (left panel) as compared with mice pre-colonized with CSAR (middle) or with CBI (right). Yellow-outlined elements indicate up-regulation of associated gene programs *in vivo*; orange indicates constitutive levels of expression, and blue down-regulation of associated gene programs. Dotted lines in the microbial cell wall indicate expression of host or microbial programs able to disrupt the pathogen's cellular integrity. Middle sections show combined effects on host inflammatory responses. Bottom sections indicate time course of *C. difficile* biomass and toxin levels, with resulting effects on host survival (bottom).